

# Regional Trends and Physical Controls of Streamflow droughts in Tropical Pluvial Flow Regimes of India

Aparna Raut<sup>1</sup>, Poulomi Ganguli<sup>\*</sup>, Rohini Kumar<sup>2</sup>, Nagarjuna N. Reddy<sup>1</sup>, Bhabani Sankar Das<sup>1</sup> and Thomas Wöhling<sup>3</sup>

<sup>1</sup>Indian Institute of Technology Kharagpur, Department of Agricultural and Food Engineering, Kharagpur, India

<sup>2</sup>UFZ-Helmholtz Centre for Environmental Research, Leipzig, Germany

<sup>3</sup>Technische Universität Dresden, Institut für Hydrologie und Meteorologie, Dresden, Germany

\*Corresponding author: P. Ganguli ([pganguli@agfe.iitkgp.ac.in](mailto:pganguli@agfe.iitkgp.ac.in))

## Key Points:

- Shifts in streamflow drought onset and deficit volume (or severity) are apparent in Peninsular river basins of India
- Nonlinear dependency between drought onset and deficit volume is observed
- Drought timing is strongly correlated to rainfall and soil moisture deficits in the eastern coastal plains of Peninsular India

## Abstract

The analysis of drought onset and their potential relationship to drought severity (deficit volume) are critical for providing timely information for agricultural operations, such as cultivation planning and crop productivity monitoring. A coupling between drought timing and deficit volume can be used as a proxy for drought-related damage estimation and associated risks. Despite its high importance, so far little attention was paid to determine the timing of drought and its linkage with deficit volume for hydrological droughts. This study utilizes quality-controlled streamflow observations from 1965 to 2018 to unveil regional patterns of hydrological drought onset, trends in event-specific deficit volume, and nonlinear relationships between onset timing and deficit volume across 97 rain-dominated catchments in Peninsular India (8-24° N, 72-87° E). Our results show a shift towards earlier hydrological drought onset in conjunction with a decrease in deficit volume during the Indian monsoon (June-September) season, which is contrasted by a delayed onset in the pre-monsoon (March-May) and post-monsoon (October-February) seasons. Further, approximately one-third of the catchments show a significant nonlinear dependency between drought deficit volume and onset time. We find environmental controls, such as soil organic carbon, vertical distance to channel network, and soil wetness are dominant factors in influencing

droughts. Our analysis provides new insights into the causal chain and physical processes linking climatic and physiographic controls on streamflow drought mechanisms, which can support drought forecasting and climate impact assessment studies.

## Plain Language Summary

In the tropics, streamflow droughts occur due to the failure of the southwest monsoon. A combination of erratic rainfall distributions and catchment-specific attributes aggravates the severity of streamflow droughts. In this paper, we analyze the change in average timing of streamflow droughts and deficit volume (severity) over Peninsular India and explore the role of physical controls on streamflow droughts. We show that during the monsoon season, a significant trend in early drought onset coincides with an increase in deficit volume. In contrast, the opposite trend is observed during the summer and winter for drought onset. A strong linkage between drought onset time and deficit volume suggests credible risk management, which requires assessment of nonlinear dependence between the interrelated attributes. To this end, we discuss the possible physical controls that drive streamflow drought dynamics. We show that while climatic controls (rainfall and soil moisture) primarily drive streamflow drought onset, physical environmental controls (catchment and terrain attributes) influence drought deficit volume together with climatic drivers. Understanding regional drivers of streamflow droughts aid in forecasting efforts and mitigation of climate change adaptation.

## 1 Introduction

Drought is a slow-onset natural hazard characterized by an extended deficit in rainfall, resulting in water shortage (Wilhite, 2005). Droughts have caused about 137 million USD damage in India between 1965 and 2019, affecting around 1.4 billion people, as reported in the Emergency Event Database in 2022 (EM-DAT, 2022). Droughts are classified into four classes such as meteorological, hydrological, agricultural and socio-economic droughts (Mishra & Singh, 2010). The abnormally low water availability in the streams is addressed as streamflow droughts. Climate change variability and change further intensify the severity of droughts (Preethi et al., 2019), gradually pushing the country to near Day Zero condition (Parvatam & Priyadarshini, 2019). Peninsular India (8-24°N, 72-87°E) is one of the significant contributors to the economy of the Indian sub-continent, such as agricultural activity, manufacturing industries, cash crops (e.g., sugarcane, 39% and cotton, 51%) and shares around 57% of the Indian population (ASG, 2019). The basin-wide surface water potential capacity of Peninsular river basins accounts for  $654.44 \times 10^9$  m<sup>3</sup>/annum, contributing ~30% of the total surface water potential of the country (IWRS, 2021). The rivers in this region of the country are rain-fed, and a large portion of streamflow occurs in the monsoon (June-September) season. Prolonged ‘breaks’ in the southwest (June-September) and/or northeastern (October-December) monsoon results in severe dry spells, *i.e.*, consecutive

days without precipitation (Mishra et al., 2021a; Raman & Rao, 1981), leading to hydrological droughts (streamflow and groundwater deficits). Peninsular India frequently experiences droughts in recent years, for example, in 2015, 2018-2019 (Bhosale and Sally, 2015; GDO, 2019; The Hindu, 2019; Sahana et al., 2020), which was triggered due to the combination of the southwest monsoon failure, unprecedented heatwaves and inadequate rainfall (GDO, 2019). Hydrological droughts are manifested by drying reservoirs, streamflow reduction, and declining groundwater levels (van Loon, 2015), over-exploitation of available water resources for irrigation and hydropower production, impacting regional food-energy-water-ecosystem resilience (Barik et al., 2017; Sanders, 2015). Further, the weakening of the monsoon in recent years (Bollasina et al., 2011; Huang et al., 2020; Kumar et al., 2020) because of global warming has increased the likelihood of persistent dry spells and hydrological droughts over Peninsular India (Bhardwaj et al., 2020; Mishra et al., 2021a).

Using well-calibrated semi-distributed Variable Infiltration Capacity-coupled-simple Groundwater Model (VIC-SIMGM), Shah & Mishra (2020) showed that the majority of hydrological drought onset in Indian subcontinent occurs during the southwest monsoon season. Droughts across Peninsular India are largely controlled by the sea surface temperature (SST) increase over the Indian Ocean (Shah & Mishra, 2020). Further, the recent multi-season drought episodes of 2016-2018 in southern India are shown to be linked with unprecedented low northeastern monsoon rainfall (Mishra et al., 2021b). Despite available literature insights into the causes of droughts (Hoerling et al., 2014; Wang et al., 2021), onset and persistence (Mo, 2011; Shah & Mishra, 2020), and frequency analyses (Chiang et al., 2018; Hoerling et al., 2011; Hoerling et al., 2012), to the best of our knowledge, analysis of co-variability between streamflow drought onset and deficit volume (severity) has until received little attention. Unlike previous drought assessments (Bhardwaj et al., 2020; Ganguli & Reddy, 2012, 2014; Shah & Mishra, 2020a; Shah & Mishra, 2016) over Peninsular India, we use high-resolution daily streamflow records for delineation of streamflow droughts that can account for strong seasonal pattern in streamflow time series (Heudorfer & Stahl, 2017a; van Loon & Laaha, 2015). The use of high-resolution temporal streamflow records enables the detection of rapid intensification/onset of catchment-scale “flash droughts,” which aid in improving seasonal-to-sub-seasonal predictability of streamflow-based droughts and devising sustainable food security policy (Pendergrass et al., 2020).

Second, little is known about whether any space-time relationship exists between timing of streamflow drought onset and the severity of the event. Understanding of drought onset and shift in its time of occurrence is especially crucial for Peninsular India, where the agrarian economy is highly dependent on rainfall distribution. Although a recent study investigated changes in dry spell duration and their timing using station-based in-situ observation at a global scale (Breinl et al., 2020), none of the assessments have investigated changing patterns of streamflow drought onset, deficit volume, and the dependence between the two drivers. In particular, it remains unclear

whether streamflow drought seasonality is the dominant driver of the severity of droughts at the tropical rain-fed catchments (van Loon and Laaha, 2015; van Loon, 2015). Third, very few assessments are available on understanding environmental controls (soil moisture, soil and catchment properties) on streamflow droughts at a regional scale, although assessment of soil and catchment properties on streamflow droughts exists in the literature (van Loon & Laaha, 2015; Ganguli et al, 2022). Since the seasonality of rainfall primarily mediates streamflow drought responses in Peninsular India (Cook et al., 2010; Mishra et al., 2021b; van Loon, 2015), it is still not clear whether the timing of drought onset alters its severity. Therefore, our research seeks to answer the following questions:

- 1) What are the regional trends in the drought onset pattern and deficit volume of streamflow droughts in the Peninsular India?
- 2) Is there a clearly identifiable relationship between streamflow drought onset and deficit volume?
- 3) How are changing patterns of onset-time and deficit volume linked to various environmental controls on streamflow droughts across Peninsular India?

To address these issues, we use daily stream gauge records of 97 sub-catchments of 17 medium to large-sized river basins over Peninsular India. We find mean drought onset is clustered around late monsoon seasons (August-September) for most gauges (71%), which show persistency in onset timing. Several gauges (30%) show a delay in drought onset than that of the sites with an earlier onset, which is limited to only 9% of the catchment. Further, we identify the environmental drivers influencing drought dynamics. Overall, our observation-based assessment helps to improve understanding of multivariate attributes, drought onset and severity, and their changes at river basin scales of Peninsular India, which have implications for building resilience to extreme droughts in the future.

## 2 Data and Methods

### 2.1 Data

We collect daily streamflow records of over five decades (1965 – 2018) from 97 catchments of Peninsular India available at the India-Water Resource Information System (India-WRIS) archive. Peninsular India (8-24° N, 72-87° E) covers nearly half of the Indian terrain with diverse topology and climate (Figure 1). To screen quality-controlled streamflow records, we apply the following criteria: (1) basins with at least a catchment area of 1000 km<sup>2</sup> or larger; (2) available record lengths of 20 years or more (3) at least 70% of daily discharge records availability. Based on these criteria, we initially selected 97 stream gauges (Table S1) from 17 large major river basin systems of Peninsular India (Figure 1).

Further, as a first-order assessment of possible anthropogenic impacts on streamflow variability, we analyze the correlation between annual average rainfall and annual mean discharge. For this, we collected high-resolution ( $0.25^\circ$ ) daily precipitation records archived at the India Meteorological Department (IMD; Pai et al., 2014). We download the gridded rainfall records for the period 1965-2018, the same length as the streamflow records, and then compute catchment-averaged rainfall time series. We obtain the monthly soil moisture records (at a depth of 1.6m; Dool et al., 2003) from the Climate Prediction Center (CPC; <https://psl.noaa.gov/data/gridded/data.cpcsoil.html>) available at a  $0.5^\circ$  spatial resolution. We use catchment boundaries available at the Global Streamflow and Meta data Archive (GSIM I; Do et al., 2018) for delineation of river basins.

Figure 1a shows the locations of stream gauges within each catchment. The Figure S1 shows the period of year-wise streamflow record availability. Selected basins are not affected by any major surface irrigation projects and dams. The fraction of area under surface irrigation for the finally selected catchments lies within the range of 0.95%-15.2% with a median value of 5.6% (MoA, 2021). We obtain soil property from the Digital Soil Maps (DSM) of India (Reddy et al., 2021a). DSM was developed based on Indian legacy soil database obtained from various archives such as the National Bureau of Soil Survey and Land Use Planning (ICAR-NBSS&LUP: <https://nbsslup.icar.gov.in/>) and other organizational publications (Reddy et al., 2021b). We retrieve soil properties at two different depths: 30 cm (weighted average of depths 0-5, 5-15, 15-30 cm) and 100 cm (weighted average of depths 0-5, 5-15, 15-30, 30-60, 60-100 cm) for the study catchments. We determine the catchment properties using the digital elevation model (DEM) archived at the Shuttle Radar Topographic Mission (SRTM) at a spatial resolution of 90 m (Jarvis et al., 2008).

## 2.2 Methods

First, we collect daily streamflow time series and precipitation records for the selected stream gauges. Since selected basins are non-perennial and rain-fed in nature, the relationship between rainfall and runoff records are considered as a deciding factor to select basins for further analyses. The workflow has several steps, such as, developing flow duration curve (FDC), comparing annual rainfall and runoff responses considering the water year (1<sup>st</sup> June – 31<sup>st</sup> May). For analysing the FDC, the flow records are split into two periods, the pre-versus the post-2000s: 1965-1999 and 2000-2018 (Figure S2). Finally, we analyze the double mass curves by establishing a graphical relationship of accumulated rainfall depth versus accumulated discharge to identify cumulative departures from the mean (Figure S3). However, analyzing the graphical relationship of rainfall depth versus the discharge of all 97 sites is a non-trivial task; hence, we consider a quantitative assessment by establishing a non-parametric association between annual average rainfall and annual mean discharge to discard gauges with possible human alterations. The annual time scale avoids the influence of inter-annual variability, affecting the rainfall-runoff relationship. We assess

the degree of association between annual average streamflow and annual mean precipitation for the whole analysis period using Kendall's rank correlation coefficient, tau ( $\tau$ ), which measures the similarity or difference of temporal patterns of the two time series (Kendall, 1938). We discard those stations (Table S2) where Kendall's  $\tau$  dependence between mean annual rainfall and runoff is less than 0.05. Finally, we selected 82 stations. Figure 2 shows the overall workflow of the analyses.

### 2.2.1 Streamflow Drought Identification

The streamflow records often contain missing values, which we infilled using time series interpolation (Ganguli & Ganguly, 2016). We identify streamflow drought using a daily variable threshold approach, where we compute the variable threshold using the 20<sup>th</sup> percentile discharge threshold (the 20<sup>th</sup> percentile flow represents the flow that is equaled or exceeded for 80% of flow records, often represented by  $Q_{80}$ ) for each day, determined using a centered moving average window of 30 days (Heudorfer and Stahl, 2017; van Lanen et al., 2013; Brunner, 2021). We implemented centered moving window through convolution operation available in MATLAB computing environment. Next, we obtain different threshold values for each calendar day of the year (considering leap year) for each catchment. We then identify drought events when consecutive daily flow values remain below the variable thresholds continuously over a period of at least 30 days. We identify drought characteristics, deficit volume as the cumulative sum of the streamflow volume lower than the variable threshold throughout the duration of the event.

### 2.2.2 Determining Mean Onset of Drought

We obtain the onset day based on Gregorian calendar (Julian date), which is then transformed into circular variable using the Eq.1. The onset date ( $J_i$ ) can be then converted to an angular value ( $\theta_i$ ), in radians for an event " $i$ " using the following relationship:

$$\theta_i = J_i \frac{2\pi}{L} \quad (1)$$

where,  $J = 1$  for January 1 and  $J = 365$  for December 31 (or 366 for leap year);  $L$  is the number of days in a year, *i.e.*, 365 for a normal year and 366 for a leap year. Next, we categorized drought events into different seasons, pre-monsoon (March-May), monsoon (June-September), and post-monsoon (October to the following year February), based on their occurrence dates. We further describe the method to determine the mean onset day and corresponding regularity (*i.e.*, seasonality) in the supplementary information, S1.1.

### 2.2.3 Analysis of Linear versus Circular Trends

For computing changes in deficit volume and event duration, we applied the simple Theil-Sen slope estimates (Sen, 1968). To make trends comparable for different catchment sizes and

climatology, we report the trend using percentage change per year by normalizing the climatology of the index time series during the analysis period (Gudmundsson et al., 2019). For computing changes in onset day, we applied Theil-Sen slope estimates with the correction for circular nature of the data. The slope estimates ( $\beta$ ) is the median of difference of dates over all possible pairs of years ( $i$  and  $j$ ) within the time series (Blöschl et al., 2017).

$$\beta = \text{median} \left( \frac{D_j - D_i + k}{j - i} \right) \quad (2)$$

$$\text{with } k = \begin{cases} -\bar{m}, & \text{if } D_j - D_i > \frac{\bar{m}}{2} \\ \bar{m}, & \text{if } D_j - D_i < -\frac{\bar{m}}{2} \\ 0 & \text{otherwise} \end{cases} \quad (3)$$

$$\bar{m} = \frac{1}{n \sum_{l=1}^n L} \quad (4)$$

Where  $\bar{m}$  is the average number of days per year,  $D_j$  and  $D_i$  are the onset time (Julian date) in time periods,  $j$  and  $i$  ( $j > i$ ) respectively. Here, if there are  $n$  values of data in the time series, it results in as many as  $N = {}^nC_2$  number of slope estimates, *i.e.*,  $\beta$  values with units of days per year. The parameter,  $k$  in Eq. 3 adjusts the circular nature of dates because the difference in event dates cannot be greater than the number of days associated with half a year.

#### 2.2.4 Spatial Synchronicity in Drought Onset versus Deficit Volume

The onset of drought is a circular variable but the deficit volume is a linear variable. For assessing the relationship between linear and circular variable, a circular-linear correlation method is utilized, which is different from typical correlation measures, such as Pearson's correlation or Kendall's  $\tau$ . The circular-linear correlation values lie between 0 and 1, where no negative correlation exists between two underlying drivers. We have considered both a parametric and a non-parametric correlation methods in our analysis.

##### • Parametric method

In the parametric approach, it is assumed that the linear variable,  $X$  (*i.e.*, deficit volume) is normally distributed and the expected value of  $X$  depends on the circular variable,  $\theta$  (here, drought onset time) with a constant variance. Second, it is assumed that  $n$  pairs of observations are mutually

independent. In particular, the expected value of  $X$  is assumed to be a function of angular distance between the angle  $\theta_0$  (direction of maximum effect) (Lototzis et al., 2018; Maridia, 1972).

In this case, the correlation coefficient between the linear variable,  $X$  and the circular variable,  $\theta$  (denoted by  $r_{X\theta}$ ) is defined as the (non-negative) square root of  $r_{X\theta}^2$ ,

$$r_{X\theta}^2 = \frac{r_{XC}^2 + r_{XS}^2 - 2r_{XC}r_{XS}r_{CS}}{1 - r_{CS}^2} \quad (5)$$

where  $r_{XC}, r_{XS}$  are respectively the partial correlation coefficient of  $X$  with  $C$  and  $S$  representing the cosine and the sine function of the angle,  $\theta$ . The  $r_{CS}$  is the correlation among the cosine and sine function of the angle.

If  $X$  and  $\theta$  are independent and  $X$  is normally distributed, then the Eq. (5) will follow a  $F$ -distribution with  $n-3$  degrees of freedom. The statistical significance of this relationship can be assessed by the following equation:

$$\frac{(n-3)r_{X\theta}^2}{1 - r_{X\theta}^2} \quad (6)$$

#### • Non-parametric method

In this method, the rank of the data is being used to find the circular-linear association. The linear variable  $X$  here is the deficit volume arranged in an ascending order  $X_1 \leq X_2 \leq X_3 \leq \dots \leq X_n$ . If  $r_1, \dots, r_n$  are the circular ranks for the drought onset time, and  $\theta_1, \dots, \theta_n$  are the corresponding ranks of the variable, then the uniform scores allotted to each of these variables are represented by  $\alpha_1, \dots, \alpha_n$

$$\alpha = \frac{2\pi r_i}{n} \quad (7)$$

Finally, the linear-circular rank correlation coefficient is defined as  $U_n$  (Maridia, 1972)

$$U_n = \frac{24(C^2 + S^2)}{n^2(n+1)} \quad (8)$$

with,  $C = \sum_{i=1}^n i \cos \alpha_i$  and  $S = \sum_{i=1}^n i \sin \alpha_i$

$U_n$  have no particular range so it is important to have a correlation coefficient to lie in the range of  $[0,1]$ . This is known as scaled correlation coefficient and is represented as  $D_n$ . (Maridia, 1972)

$$D_n = a_n(C^2 + S^2), \quad (9)$$



$$268 \quad \text{where,} \quad a_n = \begin{cases} \frac{1}{\{1+5\cot^2(\frac{\pi}{n})+4\cot^4(\frac{\pi}{n})\}}, & n \text{ even} \\ \frac{2\sin^4(\frac{\pi}{n})}{\{1+\cos(\frac{\pi}{n})\}^3}, & n \text{ odd} \end{cases}$$

269 Further, we assess the significance of the non-parametric relationship by bootstrap resampling with  
 270  $N = 1000$  iterations.

271

## 272 **2.2.5 Identification of Drought Clusters**

273 Finally, we detect the drought onset-severity hotspots within Peninsular India using a Density-  
 274 based clustering with Noise algorithm (DBSCAN; Hahsler et al., 2019), which is robust towards  
 275 outliers. Typically DBSCAN requires only two parameters, epsilon,  $\epsilon$  and the minimum points,  $p$ ,  
 276 where  $\epsilon$  indicates the radius from the core point and  $p$  is the minimum number of points that should  
 277 be considered in each cluster. We consider ranges of attributes for regionalization, such as latitude  
 278 and longitude of gauges, average annual rainfall (mm), non-parametric dependency  $D_n$ , average  
 279 deficit volume (mm), mean onset day and subsurface storage of the catchment. We calculated the  
 280 catchment-wise Baseflow Index ( $BFI$ ), which is the ratio of baseflow volume to total streamflow  
 281 volume (WMO, 2008), and used it as a proxy for the subsurface catchment storage.

282

## 283 **2.2.6 Determining Environmental Controls on Streamflow Droughts**

284 We investigate the environmental controls on streamflow drought onset and deficit volume using  
 285 catchment averaged soil moisture time series for identified drought cluster. While a complete or  
 286 partial failure of monsoon primarily causes droughts and largely controls severity of events in  
 287 India (Cook et al., 2010; Zachariah et al., 2020), the temporal variability of soil moisture influences  
 288 intensity and onset (Liang & Yuan, 2021; Zeri et al., 2022). To investigate the role of other physical  
 289 controls on streamflow droughts, we consider 4 soil signatures and 11 catchment-specific  
 290 signatures (Table S3; Beven, 2011; Wlostowski et al., 2021). To uncover dominant environment  
 291 controls on streamflow droughts, we present a graphical assessment measure, Taylor Diagram  
 292 (Taylor, 2001) for each drought cluster. Taylor Diagram compares influence of each of drivers  
 293 against the reference variable (here drought characteristics, onset and deficit volume) using  
 294 Pearson correlation coefficient, root-mean-square-deviation (RMSD), and standard deviation. To  
 295 quantitatively evaluate the influence of each static control on droughts, we use Taylor Skill Score  
 296 (TSS) and pattern Kendall's  $\tau$  dependence metrics. While pattern Kendall's  $\tau$  correlation  
 297 coefficient quantifies the similarity or difference in spatial patterns of two series, i.e., regional  
 298 drought deficit volume versus static controls, the TSS evaluates the similarity between the  
 299 distribution and amplitude of the spatial pattern of the two signals (Hirota & Takayabu, 2013;  
 300 Taylor, 2001).

$$S = \frac{4(1+R_0)}{\left(SDR + \frac{1}{SDR}\right)^2 (1+R_0)} \quad (10)$$

Where  $R$  is the pattern correlation between regional drought characteristics and static controls.  $SDR$  is the ratio of the normalized spatial standard deviations of the static controls to that of the regional drought characteristics. The term  $R_0$  indicates the maximum attainable correlation of static controls versus regional drought characteristics. As the variance of static controls approaches the variance of drought characteristics,  $R$  approaches  $R_0$  and the TSS tends to become unity. When the variance of regional drought characteristics approaches zero or the correlation value tends to become negative, TSS approaches zero value.

### 3 Results and Discussion

#### 3.1 Distribution of Streamflow Drought Onset and Persistency in Onset Timing

The mean onset of droughts is primarily clustered around the month of August and September for 71% of the catchments (Figure 3a). It confirms that streamflow droughts in peninsular catchments of India are primarily caused by prolonged dry spell and failure of the southwest monsoon (van Loon, 2015). The seasonality of droughts ranges from 0.5 to 1 (Figure 3a) – while the high seasonality (or regularity) with a value of 1 indicates persistence in drought timing, the low value 0 shows that the onset of drought is uniformly distributed throughout the year with no clear pattern. Southern India shows more variability in mean drought onset time. Summer droughts show a mean onset day clustered around April, which could be due to unavailability of pre-monsoon showers. The mean onset of events during the monsoon occurs during July to September months. In case of failure of monsoonal rainfall, the high BFI values can sustain streamflow, resulting in a delayed arrival of streamflow droughts. During post monsoon season, mean onset time typically clustered around the beginning of the season (October). The overall Kendall's  $\tau$  dependence of regularity of drought onset versus the BFI reveals a strong negative association of -0.44, significant at a 10% significance level. The second quadrant in Figure 3b (right panel) shows catchments with high regularity and low BFI. The catchments with low BFI indicates rivers are associated with small catchment memory due to less permeable soils with low soil water storage capacity, resulting in high persistence in drought onset time (Rumsey et al., 2015; Salinas et al., 2013; Yaeger et al., 2012).

The spatial distribution of frequency (number of events) of droughts for the whole year without considering seasonal stratifications suggests that overall central India is characterized with a larger number of drought events (Figure S4a). When considering individual seasons, more streamflow drought events are apparent during post-monsoon season as compared to the pre-monsoon and monsoon seasons (Figure S4b). This could be probably linked to dry winter months (3<sup>rd</sup> week December-March) when monsoon winds retreat and cold, high-pressure air mass over northern Asia moves towards the equator (Webster, 1981).

### 3.2 Temporal Shifts in Drought Onset and Deficit Volume

Next, we investigate trends in streamflow drought onset and deficit volume. Considering no seasonal stratifications for the whole year (Figure 4a-b, left panel), we find around 30% catchments show a significant delay in drought onset that ranges from 1 to 10 days per year over the period of 1965-2018. The delayed arrival of streamflow drought is compounded by a decreasing deficit volume over 20% of the peninsular catchments. Possible mechanisms that drive shift in onset time of drought and trends in deficit volume are large scale shifts in monsoon-driven precipitation (Guimbertau et al., 2012; Loo et al., 2015; Marvel et al., 2019), intensification in localized extreme rainfall events (Katzenberger et al., 2021; Krishnan et al., 2016a; Roxy et al., 2017a) and changes in evapotranspiration rate (Aadhar & Mishra, 2020; Padrón et al., 2020; Willett et al., 2007).

While the seasonal stratification shows a earlier onset of monsoon droughts with decreasing trends in deficit volume, the non-monsoonal (*i.e.*, summer and winter) droughts present a completely contrasting patterns (Figure 4): more fraction of gauges show a delayed drought onset. The drying trend is more prominent across the catchments of Krishna and Cauvery River basins (*i.e.*, the Southern part of Peninsular India). In contrast, an apparent wetter trend prevails across north and north-east Peninsular India in monsoon season (Figure 4, lower panel). This is in agreement with earlier findings, which reported monsoonal weakening in recent decades significantly enhances localized intense rainfall events, for example, in the core monsoon zone ( $18^{\circ}$ – $28^{\circ}$  N and  $73^{\circ}$ – $82^{\circ}$ ) of the country (Singh et al., 2014, Krishnan et al., 2016; Roxy et al., 2017). More irrigation and the type of irrigation in the northern India modifies the intra-seasonal properties of monsoonal precipitation, causing delayed arrival of droughts (Devanand et al., 2019).

The inter quartile range of the shift in onset varies within  $\pm 2$  days, likewise, changes in the deficit volume ranges from -1.7% to 1.2%. Our findings, overall decreasing trend in deficit volume (Figure 4b) contrasts with earlier assessments (Gudmundsson et al., 2019; 2021) that showed an increasing trend in low flows across Peninsular Indian river basins in observations and climate model simulations (see Figure 1 in Gudmundsson et al., 2021). However, in earlier assessments (Gudmundsson et al., 2019; 2021), low flows were detected by following a constant threshold approach, which was applied for the entire year irrespective of considering seasonal variability. To summarize, we find that the variable threshold credibly captures the seasonality in the drought onset pattern and the deficit volume, which was not precisely reported in earlier assessments (Gudmundsson et al., 2019; 2021), relied on constant threshold methods to detect low flow trends.

### 3.3 Asymmetrical Shift toward Stronger Dependency of Onset Time versus Deficit Volume

To determine the strength of dependency between the onset time and deficit volume, we implemented linear-circular dependence metrics (Eqs. 5 and 9). We find spatially coherent pattern

(Figure 5) among different dependence metrics with strong dependence strengths ( $D_n > 0.6$ ) across Vaitarana, Pennar, Periyar, Baitarani, 50% of Brahmani, 50% of Bharatpuzha, 45% of Krishna, 29% of Cauvery, 18% of Narmada, 20% of Godavari, and 12% of Mahanadi River basin, whereas weaker dependence strengths ( $< 0.4$ ) across Vaigai, 29% of Cauvery, 18% of Narmada, 9% of Krishna, 5% of Godavari River basin. While the values of parametric dependency vary between 0.14 and 0.98, the non-parametric dependency varies between 0.13 and 0.99. In both metrics, more than half of catchments show dependency strengths higher than 0.5 (*i.e.*,  $\sim 58\%$  in parametric and  $74\%$  in non-parametric dependence), indicating stronger positive dependency between onset time and deficit volume.

The probability density function (PDF) comparison of spatial footprints of parametric versus non-parametric dependence strengths show a significant (two-sample Kolmogorov-Smirnov test) rightward shift with an extended right tail. The asymmetrical shift towards stronger dependence is more prominent for non-parametric dependence measure as clearly depicted in the rightward shift in median with dependence strengths of more than 0.6. This suggests water resources manager should consider the adverse impact of non-linear dependence between drought onset time and deficit volume while planning, which may aid in understanding how the timing of droughts would alter event-specific severity.

### 3.4 Regionalization of Droughts Considering Spatial Coherency in Drought Onset versus Deficit Volume

The spatial distribution of drought onset versus deficit volume dependence (Figure 3) provides information on river basins that show a close correspondence between drought deficit volume and its onset time. Next, we performed regionalization of streamflow droughts using density-based spatial clustering (Hahsler et al., 2019b). The sites are then classified into three distinct regimes. Figure 6 depicts general characteristics of spatial variability of streamflow droughts classified based on a suite of geospatial and hydrometeorological attributes, such as geospatial locations of gauges, linear-circular dependency of drought attributes, basin-wide mean rainfall and subsurface storage property manifested by the BFI (see Methods). A few gauges overlap spatially among different regions due to similar hydrometeorological and geomorphological attributes.

The Region 1 contains 50 sub-catchments (the location of the flow gauging stations are shown in Figure 6a) and includes large river basins across central India (northern peninsular), such as Godavari and Narmada. The Region 1 contains the highest number of catchments and has a moderate (5.36 mm) median deficit volume with a high variance (Figure 6b). The median rainfall (Figure 6c) in this region is the highest (1189.2 mm) as compared to other regions with mean drought onset days clustered around August – September with high variability in onset time

(Figure 6b). The low BFI (Figure 6c) in this area could possibly be the reason for a high regularity in drought onset in this region.

Region 2 contains 13 sub-catchments, whereas Region 3 contains the least number of sub-catchments, i.e., 10. Region 2, where the majority of gauges are clustered around eastern coastal plains and a few gauges around southern coastal plains, shows a higher median deficit volume as compared to the other two regions (Figure 6c). Despite relatively higher BFI at Region 2, the high deficit volume at Region 2 is due to the low average rainfall. Interestingly, catchments in Region 2 show the strongest dependence strengths of onset time versus deficit volume, indicating that mean onset time, which varies from mid-August to the beginning of October (*i.e.*, monsoon drought), possibly drives the high deficit volume.

The mean onset time and deficit volume of droughts at Region 3 show a large variability as indicated by a wider temporal spread in onset time (Figure 6b) and a large interquartile range in the deficit volume (Figure 6c). However, Region 3 shows low variability in annual average rainfall. The mean onset time of droughts ranges from the middle of August to the beginning of November with a large concentration of mean onset time in the September. Region 3 is characterized by the lowest median BFI with a large variability in baseflow, indicating presence of impermeable basin geology with a flashy catchments (*i.e.*, steep rising limb of the hydrograph with a small lag-time). Interestingly, rivers in this regime show the lowest dependence strengths of onset time versus deficit volume, although they exhibit the highest regularity (Figure 6b-c). A few catchments in this regime show a mean drought onset time between October and November with regularity values greater than 0.5 to close to 1. To summarize, rivers in Region 3 have the least groundwater recharge; the failure of both southwest and northeast monsoon drives streamflow droughts for this regime. Our findings are in agreement with an earlier study (Mishra et al., 2021b) that showed moderate-to-exceptionally low northeastern monsoon in recent years driving severe droughts and water scarcity in southern India.

Taken together, aggregating all three regimes, we find that the mean drought onset is in September for more than 41% of gauges. The interquartile ranges of mean drought deficit volume and dependence strengths for these gauges vary from 2.8-6.2 mm and 0.62-0.73, respectively. In contrast, only 19% of catchments show the mean drought onset around the middle of October and the beginning of November and these are primarily clustered around the southern part of Peninsular India. The interquartile ranges of mean drought deficit volume and dependence strengths of these catchments varies from 2.2-4 mm and 0.41-0.68, respectively. This implies that monsoon drought is slightly more severe as compared to post-monsoon droughts in Peninsular India. Severe monsoon droughts possibly result from the concurrence of heatwaves and dry spells, which intensifies land-atmosphere feedback, leading to unprecedented low soil water regime over

large areas, moisture limitations suppressing cloud formation, and increased temperatures in a multi-week episode (Dirmeyer et al., 2021; Miralles et al., 2019; Panda et al., 2017). Next, we assess inter-regional differences in bivariate drought properties, i.e., dependence strengths of mean onset time versus deficit volume using Wilcoxon rank sum test (Kim, 2014). Our analyses show that inter-regional differences across clusters are statistically indistinguishable considering dependence strengths between onset time of streamflow droughts and corresponding deficit volume (see the supplementary information, S1.2 for details).

### 3.4 Assessing Streamflow Droughts with Environmental Controls

To understand climate and physiographic controls on streamflow droughts, first we investigate the temporal variability of soil moisture relative to drought deficit time series during 1980-2018. As the soil moisture shows the integrated effect of rainfall, temperature and other metrological parameters, we have chosen this variable to access the environmental controls. The temporal evolutions of streamflow droughts follow asynchronous variability of soil moisture – high (low) soil moisture leads to low (high) deficit volume (Figure 7), which strongly suggests a causal link. A pronounced lag effect between soil moisture and deficit volume is often apparent due to its memory effect (Wilby et al., 2004). The deeper layer of soil moisture (as here) evolves slowly and supports drought monitoring (NOAA, 2022). The inter-annual variability is prominent in soil moisture versus the deficit volume time series. For example, in Region 1, soil moisture observations show an increasing wet pattern during the epoch (1990 – 2000), which could be associated with an increasing wet spells and reduced number of drought years in central India after 1980s (Sahoo & Yadav, 2022). Typically, Region 1 contains a few severe outlying drought events with large deficit volume (i.e., > 15 mm) during the years 1983, 1987, 2002 and 2009, which were typically associated with large-scale climatic “teleconnection” pattern, El Niño events. Precipitation in India is known to be linked with large-scale teleconnections through sea surface temperature (SST), which induces large-scale atmospheric patterns triggering the development of dry spells and monsoon failures, resulting in severe droughts/dry spells (Mooley & Parthasarathy, 1983; Pai et al., 2017; Schulte et al., 2020). The concurrences of heatwaves and drought in 2002 and 2009 (Gadgil et al., 2004; Panda et al., 2017), resulted in crop failures, depletion in surface and subsurface water availability, shortages in power production, and overall huge economic losses of ~1% of gross domestic production in 2002.

In Region 2, the median of weighted average deficit volume of all events remains the highest nearing 7.4 mm (Figure 7, middle panel). A time lag typically exists between soil moisture and deficit volume with recovery from baseflow, possibly due to higher sand content in the eastern coastal plain (Rumsey et al., 2015), which slows down the development of droughts and lowers deficit volume. This could be attributed to highly permeable soil layers (Kelly et al., 2020) in this region as manifested by the high BFI of catchments (Figure 6c). In Region 3, the soil moisture is

generally higher than that of the other two regions. The deficit volume in this region shows high variability. After 1990, we find a sharp drop in drought deficit volume in Region 3, which is contrasted by an increase in the soil moisture. Drought during the year 2000-2003 was severe as reported in several studies (Bhat, 2006; Mishra, 2020); especially during the year 2002, India incurred a total damage of 8.3 Million USD, which affected around 300 million people (EM-DAT, 2022). The severe drought of 2002 is well captured in all three regions as depicted by low soil moisture during this period.

While climatic properties, *e.g.*, soil moisture influences drought onset, both climatic (soil moisture) and catchment (catchment, topographic, and soil) properties have a key role in determining the deficit volume. Once environmental controls are analyzed against the drought characteristics, we refer to them as (potential) covariates. We identify the influence of static environmental controls (Table S3) on streamflow droughts using Taylor diagrams and Taylor Skill score (See Methods). The Taylor diagram demonstrates the skill of static environmental controls in mediating drought deficit volume using a set of performance measures, such as standard deviation, RMSD, and centered pattern correlation coefficients relative to the index series, *i.e.*, region-wise station-based drought deficit volume in a single plot (Figure 8). We find that the static environmental controls have trivial influence on timing of drought onset as manifested by very low TSS that varies from 0 to 0.046 for all three regions. Out of three regimes, Region 1 shows the least skill (the maximum TSS value of 0.004). Although Regime 1 shows very low pattern *linear-circular* correlation coefficients for onset time versus static environmental controls ( $D_n = 0.003 \dots 0.09$ ), for the other two regimes, the correlation is relatively higher and varies from 0.09 to 0.92 (Figure S5). Typically,  $D_n$  values are larger for soil properties in Region 2 than Region 3, whereas catchment properties are strongly correlated with onset time in Region 3 (Figure S5). Among soil attributes, Soil organic carbon (SOC) and stocks at the surface and sub-surface levels are significantly correlated with onset timing, whereas among catchment attributes, aspect and slope are dominant physiographic controls for both regions.

Figure 8 shows static soil features, surface (30 cm) and sub-surface (up to 1m) soil organic stock and cation exchange capacity (CEC) are the dominant soil controls. In Region 1, organic stock is negatively correlated with drought deficit volume, indicating a low SOC content results in a high deficit volume (Figure 8a). In contrast, the TSS scores of drought deficit volume versus soil organic stock are generally high (Figure 8b) and show significant positive dependence in Region 3 (Figure 8a). This might be due to soil texture and structure that impact the permeability. The average clay and sand percentages indicate clay texture of soil over the region 3. As we move from region 1 to 3, the sand fraction decreases, but the clay fraction tends to increase (Figure S6). While regions 1 and 3 show a significant negative association with near-surface (30 cm depth) clay content versus drought deficit volume, only sub-surface (*i.e.*, 1 m deep) clay content shows a significant negative association with drought deficit volume for Region 2 (Figure 8a). A negative

association between sub-surface clay content and drought deficit volume suggests at a deeper depth, soil permeability has increased gradually, which is also reflected in high BFI values in Region 2. This region has low & highly variable median CEC content with relatively high subsurface clay content (Figure S6). Interestingly, this region also has a high proportion of sand, making soils highly conductive to the flow of water. Further, across all depths, significant negative correlations are apparent for the CEC versus deficit volume, except Region 1, TSS values are low for other two regions. This implies that although there is an anti-synchronicity between the two spatial series as indicated by a robust negative pattern Kendall's  $\tau$ , a high variability exists in the drought deficit volume relative to the index series, *i.e.*, soil CEC (Figure 8a). The soil CEC helps soil to hold nutrients, organic matter contents and buffer pH, and thus plays a crucial role in maintaining soil structure and further aids in tolerance of vegetation towards drought (Ruiz Sinoga et al., 2012; Fang et al., 2017; Lukowska & Józefaciuk, 2016). Soils with low CEC may show low water holding capacities leading to quick drying, compounding streamflow drought deficit volume, which may possibly explains the negative association between these two variables. Region 2 has the highest average deficit volume, which is supported by the lowest median CEC (Figures 6 and S6).

Likewise, catchment properties, such as topographic ruggedness index (TRI), slope, topographic wetness index (TWI), vertical distance to channel network (VDCN), and longitudinal curvature are found to be dominant physiographic covariates controlling the streamflow drought deficit volume. The TSS values of dominant catchment-specific attributes versus drought deficit volume varies from 0-0.53 with pattern Kendall's  $\tau$  from -0.69 to 0.59. However, a few physiographic attributes do not show any substantial association with deficit volume, such as aspect, convergence index, hillshading and relative slope. The catchment properties, slope, TRI and cross sectional curvature shows significant positive correlation with deficit volume, whereas the long curvature shows negative correlation. The environmental covariate, VDCN shows the largest TSS score relative to the deficit volume. VDCN enhances the vegetative yield, in turn more water availability for plants enhancing soil SOC (Horst et al., 2018). The slope, terrain curvatures, and topographic heterogeneity, indicated by the TRI, influence catchment-related hydrological responses driving flow direction, water accumulation, runoff velocity and soil moisture, therefore, play a vital role in regulating water availability in a catchment (Amatulli et al., 2018). Figure S7 shows the variability in dominant catchment properties across different regimes. The TWI is commonly used as a proxy for soil moisture distribution and measure terrain-driven balance of the catchment water supply and local drainage (Kopecký et al., 2021; Raduła et al., 2018), which drives the negative correlation of TWI against streamflow deficit volume. The lowest median TWI (Figure S7) and low median soil moisture values (Figure 7) across Region 2 are responsible for the highest median drought deficit volume. Overall our findings aid in understanding the causal chain of physical



processes, linking climatic and physiographic controls on streamflow droughts. Further, it helps in understanding tropical climate response to water availability in a changing climate.

#### 4. Summary and Conclusions

In this paper, we proposed a data-driven analysis to quantify streamflow droughts and analysed their space-time clustering patterns over Peninsular India. We investigated catchment-wise onset patterns and explored the relationships between bivariate drought characteristics, the timing of drought onset, and event-specific deficit volume using *circular-linear* dependence metrics. The analyzed physiographic controls include variables related to the antecedent catchment wet-/dryness manifested by soil moisture, soil and topographic characteristics, and event-specific characteristics, such as the onset timing and dependence between drought onset and deficit volume. Using quality-controlled river discharge records from streamflow gauges covering Peninsular India, we proposed a methodology to (a) find the spatial distribution of persistency in the timing of drought onset; (b) identify shifts in the mean timing of droughts and deficit volume that expose disparate trends considering seasonal stratifications; (c) use *circular-linear* dependence metrics not only to identify temporal coherency between drought onset and event-specific deficit volume across individual catchments but also to identify spatial drought clusters to detect vulnerable areas where onset timing is closely related to the severity of events. The key insights from our study can be summarized as follows:

- We show a statistically significant relationship between the onset timing of streamflow droughts and event-specific deficit volume across river basins of Peninsular India and detected temporal synchronicity in onset timing. In addition, we find an inverse relationship of persistency in the timing of streamflow drought (i.e., regularity) versus the BFI, a proxy for catchment sub-surface water storage.
- The analysis of trends in streamflow drought onset timing and deficit volume by season show a disparate pattern between monsoon and non-monsoon events. A significant shift to an earlier onset of monsoon drought is observed which is associated by a decrease in deficit volume for most of the catchments, whereas the pre-monsoon and post-monsoon seasons show an delayed drought onset. The contrasting trends in drought onset versus deficit volume in the monsoon season are linked to monsoonal weakening in recent decades, substantially enhancing localized extreme rain events (Krishnan et al., 2016; Roxy et al., 2017).
- Our observational evidence shows a strong coherence between streamflow drought onset time and deficit volume (severity) in several peninsular catchments and particularly in the Krishna River basin. Our assessments suggest that the timing of drought onset plays a central role in controlling drought deficit volume in the pluvial discharge regime. For the

first time, we show that streamflow drought onset and deficit volume co-vary and often show synchronicity in space-time.

- We identified three distinct drought clusters based on similarity measures of hydrometeorological attributes. Drought onset in Region 1 is temporally clustered around August – September. The high rainfall pattern in this region results in a moderate deficit volume of droughts, although there is evidence of a few severe outlying events. In contrast, Region 2 shows the highest average deficit volume, which is associated with low annual average rainfall distribution. Furthermore, catchments in Region 3 show the lowest subsurface storage with a high variability because of low BFI values, which may result in a highly regular drought onset time.
- The association of static physiographic signatures with onset time showed robust *linear-circular* correlation for all catchments except for region 1. Soil attributes such as organic stocks are significantly correlated to the onset time for both regions 2 and 3. These properties strongly mediate drought deficit volume in all three regions, while the strength varies from low to high across Region 1 to Region 3. A robust skill score is apparent for sub-surface stock versus deficit volume for Regions 2 and 3, whereas the skill is relatively low at Region 1. Among catchment attributes TRI, TWI, VDCN and longitudinal curvature are found to be dominant physiographic attributes controlling the streamflow drought deficit volume.
- The dependence of drought onset and deficit volume and evidence of causal interactions between catchment-scale droughts and physiographic signatures provides the possibility of developing drought early warning tools and improving probabilistic assessment of drought risks by linking it to hazard frequency. The drought hazard assessment considering onset timing as a conditioning driver could help to enhance probabilistic prediction of seasonal to sub-seasonal low flows and inform timely forecast.

Our analysis is purposefully limited to rain-fed catchments across Peninsular India. The effect of snow-melt in drought propagation is negligible here, and our analysis focused on an integrated aspect of streamflow droughts resulting from precipitation variability. Second, it has been widely acknowledged that the onset of drought is associated with anomalous moisture transport linked to large-scale atmospheric-ocean teleconnection (Emerton et al., 2019; Ionita & Nagavciuc, 2020). Investigations of dominant modes of teleconnection patterns (Azad & Rajeevan, 2016; Dutta & Maity, 2020), namely El Niño-Southern Oscillation (ENSO) and the Equatorial Indian Ocean Oscillation (EQUINOO), on shifts in drought timing and its catchment-specific responses requires a separate in-depth analysis. Nevertheless, we like to stress that the derived insights would enhance seasonal to sub-seasonal streamflow drought forecasts and risk management, essential for water managers and stakeholders coping with water stress, especially in regions or seasons with low drought predictability. Moreover, the process-informed statistical framework presented here

would also benefit the prediction of other hydroclimatic extremes, such as floods and wildfire (Do et al., 2020; Engström et al., 2022).

## Acknowledgments

Aparna Raut is supported by PMRF, Govt of India scholarship for Doctoral studies at IITs. Poulomi Ganguli is supported through Science and Engineering Research Board, Government of India's early career start-up grant, SRG/2019/000044. The financial support from German Academic Exchange Service (DAAD), under the program "Combined Study and Practice Stays for Engineers from Developing Countries (KOSPIE) with Indian IITs, 2020" (ID: 57525292) is highly acknowledged. The first author would like to thank Bhupinderjeet Singh, doctoral student at University of Washington at Pullman for the fruitful discussions on method to compute baseflow index from daily streamflow records.

## Open Research

The streamflow data is obtained from India-Water Resource Information System (India-WRIS, <https://indiawris.gov.in/wris/#/>). The precipitation data is retrieved from the daily precipitation records archived at the India Metrological Department (IMD, [https://www.imdpune.gov.in/Clim\\_Pred\\_LRF\\_New/](https://www.imdpune.gov.in/Clim_Pred_LRF_New/)). We obtain the monthly soil moisture records from the Climate Prediction Center (CPC; <https://psl.noaa.gov/data/gridded/data.cpcsoil.html>) available at a 0.5° spatial resolution. We use catchment boundaries available at the Global Streamflow and Meta data Archive (<https://doi.pangaea.de/10.1594/PANGAEA.887477>). The digital soil mapping for India was developed using an Indian soil legacy database that utilized archived data from various sources, such as the National Bureau of Soil Survey and Land Use Planning (NBSS&LUP; <https://www.nbsslup.in/>) and other institution publications. The MATLAB Codes used for analysis have been archived by the authors and are available on request from P.G., [pganguli@agfe.iitkgp.ac.in](mailto:pganguli@agfe.iitkgp.ac.in). The source codes for Digital Soil Map of India codes are available from authors through personal request.

## References

- Aadhar, S., & Mishra, V. (2020). Increased Drought Risk in South Asia under Warming Climate: Implications of Uncertainty in Potential Evapotranspiration Estimates. *Journal of Hydrometeorology*, 21(12), 2979–2996. <https://doi.org/10.1175/JHM-D-19-0224.1>
- Agricultural Statistics at a Glance 2019. (2019), 335.
- Amatulli, G., Domisch, S., Tuanmu, M.-N., Parmentier, B., Ranipeta, A., Malczyk, J., & Jetz, W. (2018). A suite of global, cross-scale topographic variables for environmental and biodiversity modeling. *Scientific Data*, 5(1), 180040. <https://doi.org/10.1038/sdata.2018.40>
- Azad, S., & Rajeevan, M. (2016). Possible shift in the ENSO-Indian monsoon rainfall relationship under future global warming. *Scientific Reports*, 6(1), 20145. <https://doi.org/10.1038/srep20145>
- Barik, B., Ghosh, S., Sahana, A. S., Pathak, A., & Sekhar, M. (2017). Water–food–energy nexus with changing agricultural scenarios in India during recent decades. *Hydrology and Earth System Sciences*, 21(6), 3041–3060.
- Beven, K. J. (2011). *Rainfall-runoff modelling: the primer*. John Wiley & Sons.
- Bhardwaj, K., Shah, D., Aadhar, S., & Mishra, V. (2020). Propagation of Meteorological to Hydrological Droughts in India. *Journal of Geophysical Research: Atmospheres*, 125(22), e2020JD033455. <https://doi.org/10.1029/2020JD033455>
- Bhat, G. S. (2006). The Indian drought of 2002—a sub-seasonal phenomenon? *Quarterly Journal of the Royal Meteorological Society*, 132(621), 2583–2602. <https://doi.org/10.1256/qj.05.13>

- Bhosale, J., & Sally, M. (2015, February 9). Peninsular India reeling as drought conditions worsen; rabi crop depends on September rainfall. Retrieved from <https://economictimes.indiatimes.com/news/economy/indicators/peninsular-india-reeling-as-drought-conditions-worsen-rabi-crop-depends-on-september-rainfall/articleshow/48776472.cms?from=mdr>
- Bollasina, M. A., Ming, Y., & Ramaswamy, V. (2011). Anthropogenic Aerosols and the Weakening of the South Asian Summer Monsoon. *Science*, 334(6055), 502–505. <https://doi.org/10.1126/science.1204994>
- Breinl, K., Baldassarre, G. D., Mazzoleni, M., Lun, D., & Vico, G. (2020). Extreme dry and wet spells face changes in their duration and timing. *Environmental Research Letters*, 15(7), 074040. <https://doi.org/10.1088/1748-9326/ab7d05>
- Chiang, F., Mazdiasni, O., & AghaKouchak, A. (2018). Amplified warming of droughts in southern United States in observations and model simulations. *Science Advances*, 4(8), eaat2380. <https://doi.org/10.1126/sciadv.aat2380>
- Cook, E. R., Anchukaitis, K. J., Buckley, B. M., D'Arrigo, R. D., Jacoby, G. C., & Wright, W. E. (2010). Asian monsoon failure and megadrought during the last millennium. *Science*, 328(5977), 486–489.
- Devanand, A., Huang, M., Ashfaq, M., Barik, B., & Ghosh, S. (2019). Choice of Irrigation Water Management Practice Affects Indian Summer Monsoon Rainfall and Its Extremes. *Geophysical Research Letters*, 46(15), 9126–9135. <https://doi.org/10.1029/2019GL083875>
- Dirmeyer, P. A., Balsamo, G., Blyth, E. M., Morrison, R., & Cooper, H. M. (2021). Land-Atmosphere Interactions Exacerbated the Drought and Heatwave Over Northern Europe

- During Summer 2018. *AGU Advances*, 2(2), e2020AV000283.  
<https://doi.org/10.1029/2020AV000283>
- Do, H. X., Gudmundsson, L., Leonard, M., & Westra, S. (2018). The Global Streamflow Indices and Metadata Archive (GSIM) – Part 1: The production of a daily streamflow archive and metadata. *Earth System Science Data*, 10(2), 765–785. <https://doi.org/10.5194/essd-10-765-2018>
- Do, H. X., Westra, S., Leonard, M., & Gudmundsson, L. (2020). Global-scale prediction of flood timing using atmospheric reanalysis. *Water Resources Research*, 56(1), e2019WR024945.
- Dool, van den, Huang, J., & Fan, Y. (2003). Performance and analysis of the constructed analogue method applied to U.S. soil moisture over 1981–2001. *Journal of Geophysical Research: Atmospheres*, 108(D16). <https://doi.org/10.1029/2002JD003114>
- Dutta, R., & Maity, R. (2020). Spatial variation in long-lead predictability of summer monsoon rainfall using a time-varying model and global climatic indices. *International Journal of Climatology*, 40(14), 5925–5940. <https://doi.org/10.1002/joc.6556>
- EM-DAT. (2022). The International Disaster Database. <https://www.emdat.be/database>
- Emerton, R. E., Stephens, E. M., & Cloke, H. L. (2019). What is the most useful approach for forecasting hydrological extremes during El Niño? *Environmental Research Communications*, 1(3), 031002. <https://doi.org/10.1088/2515-7620/ab114e>
- Engström, J., Abbaszadeh, P., Keellings, D., Deb, P., & Moradkhani, H. (2022). Wildfires in the Arctic and tropical biomes: what is the relative role of climate? *Natural Hazards*. <https://doi.org/10.1007/s11069-022-05452-2>
- Fang, K., Kou, D., Wang, G., Chen, L., Ding, J., Li, F., et al. (2017). Decreased Soil Cation Exchange Capacity Across Northern China's Grasslands Over the Last Three Decades.

*Journal of Geophysical Research: Biogeosciences*, 122(11), 3088–3097.  
<https://doi.org/10.1002/2017JG003968>

Gadgil, S., Vinayachandran, P., Francis, P., & Gadgil, S. (2004). Extremes of the Indian summer monsoon rainfall, ENSO and equatorial Indian Ocean oscillation. *Geophysical Research Letters*, 31(12).

Ganguli, P., & Ganguly, A. R. (2016). Space-time trends in U.S. meteorological droughts. *Journal of Hydrology: Regional Studies*, 8, 235–259. <https://doi.org/10.1016/j.ejrh.2016.09.004>

Ganguli, P., & Reddy, M. J. (2012). Risk Assessment of Droughts in Gujarat Using Bivariate Copulas. *Water Resources Management*, 26(11), 3301–3327.  
<https://doi.org/10.1007/s11269-012-0073-6>

Ganguli, P., & Reddy, M. J. (2014). Evaluation of trends and multivariate frequency analysis of droughts in three meteorological subdivisions of western India. *International Journal of Climatology*, 34(3), 911–928. <https://doi.org/10.1002/joc.3742>

GDO (Global Drought Observatory). (2019). *Drought in India – June 2019* (pp. 1–17). JRC and ERCC Analytical Team. Retrieved from  
[https://edo.jrc.ec.europa.eu/documents/news/GDODroughtNews201906\\_India.pdf](https://edo.jrc.ec.europa.eu/documents/news/GDODroughtNews201906_India.pdf)

Gudmundsson, L., Leonard, M., Do, H. X., Westra, S., & Seneviratne, S. I. (2019). Observed Trends in Global Indicators of Mean and Extreme Streamflow. *Geophysical Research Letters*, 46(2), 756–766. <https://doi.org/10.1029/2018GL079725>

Gudmundsson, Lukas, Boulange, J., Do, H. X., Gosling, S. N., Grillakis, M. G., Koutroulis, A. G., et al. (2021). Globally observed trends in mean and extreme river flow attributed to climate change. *Science*, 371(6534), 1159–1162.

- Guimberteau, M., Laval, K., Perrier, A., & Polcher, J. (2012). Global effect of irrigation and its impact on the onset of the Indian summer monsoon. *Climate Dynamics*, 39(6), 1329–1348. <https://doi.org/10.1007/s00382-011-1252-5>
- Hahsler, M., Piekenbrock, M., & Doran, D. (2019a). **dbscan** : Fast Density-Based Clustering with *R. Journal of Statistical Software*, 91(1). <https://doi.org/10.18637/jss.v091.i01>
- Hahsler, M., Piekenbrock, M., & Doran, D. (2019b). dbscan: Fast Density-Based Clustering with *R. Journal of Statistical Software*, 91, 1–30. <https://doi.org/10.18637/jss.v091.i01>
- Heudorfer, B., & Stahl, K. (2017a). Comparison of different threshold level methods for drought propagation analysis in Germany. *Hydrology Research*, 48(5), 1311–1326.
- Heudorfer, B., & Stahl, K. (2017b). Comparison of different threshold level methods for drought propagation analysis in Germany. *Hydrology Research*, 48(5), 1311–1326. <https://doi.org/10.2166/nh.2016.258>
- Hirota, N., & Takayabu, Y. N. (2013). Reproducibility of precipitation distribution over the tropical oceans in CMIP5 multi-climate models compared to CMIP3. *Climate Dynamics*, 41(11), 2909–2920. <https://doi.org/10.1007/s00382-013-1839-0>
- Hoerling, M., Eischeid, J., Perlwitz, J., Quan, X., Zhang, T., & Pegion, P. (2011). On the Increased Frequency of Mediterranean Drought. *Journal of Climate*, 25(6), 2146–2161. <https://doi.org/10.1175/JCLI-D-11-00296.1>
- Hoerling, M., Eischeid, J., Kumar, A., Leung, R., Mariotti, A., Mo, K., et al. (2014). Causes and predictability of the 2012 Great Plains drought. *Bulletin of the American Meteorological Society*, 95(2), 269–282.



- Hoerling, M. P., Eischeid, J. K., Quan, X.-W., Diaz, H. F., Webb, R. S., Dole, R. M., & Easterling, D. R. (2012). Is a transition to semipermanent drought conditions imminent in the US Great Plains? *Journal of Climate*, 25(24), 8380–8386.
- Horst, T. Z., Dalmolin, R. S. D., Caten, A. ten, Moura-Bueno, J. M., Cancian, L. C., Pedron, F. de A., & Schenato, R. B. (n.d.). Edaphic and Topographic Factors and their Relationship with Dendrometric Variation of *Pinus Taeda* L. in a High Altitude Subtropical Climate. *Revista Brasileira de Ciência Do Solo*, 42. Retrieved from <https://www.redalyc.org/jatsRepo/1802/180256032019/html/index.html>
- Huang, X., Zhou, T., Turner, A., Dai, A., Chen, X., Clark, R., et al. (2020). The Recent Decline and Recovery of Indian Summer Monsoon Rainfall: Relative Roles of External Forcing and Internal Variability. *Journal of Climate*, 33(12), 5035–5060. <https://doi.org/10.1175/JCLI-D-19-0833.1>
- Ionita, M., & Nagavciuc, V. (2020). Forecasting low flow conditions months in advance through teleconnection patterns, with a special focus on summer 2018. *Scientific Reports*, 10(1), 13258. <https://doi.org/10.1038/s41598-020-70060-8>
- Jarvis, A., Guevara, E., Reuter, H. I., & Nelson, A. D. (2008). Hole-filled SRTM for the globe: version 4: data grid.
- Katzenberger, A., Schewe, J., Pongratz, J., & Levermann, A. (2021). Robust increase of Indian monsoon rainfall and its variability under future warming in CMIP6 models. *Earth System Dynamics*, 12(2), 367–386. <https://doi.org/10.5194/esd-12-367-2021>
- Kendall, M. G. (1938). A new measure of rank correlation. *Biometrika*, 30(1/2), 81–93.

- Kim, H.-Y. (2014). Statistical notes for clinical researchers: Nonparametric statistical methods: 1. Nonparametric methods for comparing two groups. *Restorative Dentistry & Endodontics*, 39(3), 235–239. <https://doi.org/10.5395/rde.2014.39.3.235>
- Kopecký, M., Macek, M., & Wild, J. (2021). Topographic Wetness Index calculation guidelines based on measured soil moisture and plant species composition. *The Science of the Total Environment*, 757, 143785. <https://doi.org/10.1016/j.scitotenv.2020.143785>
- Krishnan, R., Sabin, T. P., Vellore, R., Mujumdar, M., Sanjay, J., Goswami, B. N., et al. (2016a). Deciphering the desiccation trend of the South Asian monsoon hydroclimate in a warming world. *Climate Dynamics*, 47(3), 1007–1027. <https://doi.org/10.1007/s00382-015-2886-5>
- Krishnan, R., Sabin, T. P., Vellore, R., Mujumdar, M., Sanjay, J., Goswami, B. N., et al. (2016b). Deciphering the desiccation trend of the South Asian monsoon hydroclimate in a warming world. *Climate Dynamics*, 47(3), 1007–1027. <https://doi.org/10.1007/s00382-015-2886-5>
- Kumar, P. V., Naidu, C. V., & Prasanna, K. (2020). Recent unprecedented weakening of Indian summer monsoon in warming environment. *Theoretical and Applied Climatology*, 140(1), 467–486. <https://doi.org/10.1007/s00704-019-03087-1>
- Liang, M., & Yuan, X. (2021). Critical Role of Soil Moisture Memory in Predicting the 2012 Central United States Flash Drought. *Frontiers in Earth Science*, 9. Retrieved from <https://www.frontiersin.org/articles/10.3389/feart.2021.615969>
- Loo, Y. Y., Billa, L., & Singh, A. (2015). Effect of climate change on seasonal monsoon in Asia and its impact on the variability of monsoon rainfall in Southeast Asia. *Geoscience Frontiers*, 6(6), 817–823. <https://doi.org/10.1016/j.gsf.2014.02.009>
- Lototzis, M., Papadopoulos, G. K., Droulia, F., Tseliou, A., & Tsiros, I. X. (2018). A note on the correlation between circular and linear variables with an application to wind direction and

- air temperature data in a Mediterranean climate. *Meteorology and Atmospheric Physics*, 130(2), 259–264. <https://doi.org/10.1007/s00703-017-0508-y>
- Lukowska, M., & Józefaciuk, G. (2016). Osmotic stress induces severe decrease in cation exchange capacity and surface groups of medium acidity in roots of cereal plants. *Acta Physiologiae Plantarum*, 38(1), 31. <https://doi.org/10.1007/s11738-015-2050-1>
- Maridia. (1972). *Statistics of Directional Data*. Elsevier. <https://doi.org/10.1016/C2013-0-07425-7>
- Marvel, K., Cook, B. I., Bonfils, C. J. W., Durack, P. J., Smerdon, J. E., & Williams, A. P. (2019). Twentieth-century hydroclimate changes consistent with human influence. *Nature*, 569(7754), 59–65. <https://doi.org/10.1038/s41586-019-1149-8>
- Miralles, D. G., Gentile, P., Seneviratne, S. I., & Teuling, A. J. (2019). Land–atmospheric feedbacks during droughts and heatwaves: state of the science and current challenges. *Annals of the New York Academy of Sciences*, 1436(1), 19–35. <https://doi.org/10.1111/nyas.13912>
- Mishra, A. K., & Singh, V. P. (2010). A review of drought concepts. *Journal of Hydrology*, 391(1), 202–216. <https://doi.org/10.1016/j.jhydrol.2010.07.012>
- Mishra, V. (2020). Long-term (1870–2018) drought reconstruction in context of surface water security in India. *Journal of Hydrology*, 580, 124228. <https://doi.org/10.1016/j.jhydrol.2019.124228>
- Mishra, V., Thirumalai, K., Jain, S., & Aadhar, S. (2021a). Unprecedented drought in South India and recent water scarcity. *Environmental Research Letters*. <https://doi.org/10.1088/1748-9326/abf289>

- 846 Mishra, V., Thirumalai, K., Jain, S., & Aadhar, S. (2021b). Unprecedented drought in South India  
 847 and recent water scarcity. *Environmental Research Letters*, 16(5), 054007.  
 848 <https://doi.org/10.1088/1748-9326/abf289>
- 849 Mo, K. C. (2011). Drought onset and recovery over the United States. *Journal of Geophysical*  
 850 *Research: Atmospheres*, 116(D20). <https://doi.org/10.1029/2011JD016168>
- 851 Mooley, D. A., & Parthasarathy, B. (1983). Indian summer monsoon and El Nino. *Pure and*  
 852 *Applied Geophysics*, 121(2), 339–352. <https://doi.org/10.1007/BF02590143>
- 853 Padrón, R. S., Gudmundsson, L., Decharme, B., Ducharne, A., Lawrence, D. M., Mao, J., et al.  
 854 (2020). Observed changes in dry-season water availability attributed to human-induced  
 855 climate change. *Nature Geoscience*, 13(7), 477–481. [https://doi.org/10.1038/s41561-020-](https://doi.org/10.1038/s41561-020-0594-1)  
 856 0594-1
- 857 Pai, D. S., Sridhar, L., Rajeevan, M., Sreejith, O. P., Satbhai, N. S., & Mukhopadhyay, B. (2014).  
 858 Development of a new high spatial resolution ( $0.25^\circ \times 0.25^\circ$ ) long period (1901–2010)  
 859 daily gridded rainfall data set over India and its comparison with existing data sets over the  
 860 region, 18.
- 861 Pai, D. S., Guhathakurta, P., Kulkarni, A., & Rajeevan, M. N. (2017). Variability of  
 862 Meteorological Droughts Over India. In M. N. Rajeevan & S. Nayak (Eds.), *Observed*  
 863 *Climate Variability and Change over the Indian Region* (pp. 73–87). Singapore: Springer.  
 864 [https://doi.org/10.1007/978-981-10-2531-0\\_5](https://doi.org/10.1007/978-981-10-2531-0_5)
- 865 Panda, D. K., AghaKouchak, A., & Ambast, S. K. (2017). Increasing heat waves and warm spells  
 866 in India, observed from a multiaspect framework: Heat Wave and Warm Spells in India.  
 867 *Journal of Geophysical Research: Atmospheres*, 122(7), 3837–3858.  
 868 <https://doi.org/10.1002/2016JD026292>

- 869 Parvatam, S., & Priyadarshini, S. (2019, July). On Day Zero, India prepares for a water emergency.  
 870 Retrieved April 1, 2021, from  
 871 <https://www.natureasia.com/en/nindia/article/10.1038/nindia.2019.84>
- 872 Pendergrass, A. G., Meehl, G. A., Pulwarty, R., Hobbins, M., Hoell, A., AghaKouchak, A., et al.  
 873 (2020). Flash droughts present a new challenge for subseasonal-to-seasonal prediction.  
 874 *Nature Climate Change*, 10(3), 191–199. <https://doi.org/10.1038/s41558-020-0709-0>
- 875 Preethi, B., Ramya, R., Patwardhan, S. K., Mujumdar, M., & Kripalani, R. H. (2019). Variability  
 876 of Indian summer monsoon droughts in CMIP5 climate models. *Climate Dynamics*, 53(3),  
 877 1937–1962. <https://doi.org/10.1007/s00382-019-04752-x>
- 878 Raduła, M. W., Szymura, T. H., & Szymura, M. (2018). Topographic wetness index explains soil  
 879 moisture better than bioindication with Ellenberg's indicator values. *Ecological Indicators*,  
 880 85, 172–179. <https://doi.org/10.1016/j.ecolind.2017.10.011>
- 881 Raman, C. R. V., & Rao, Y. P. (1981). Blocking highs over Asia and monsoon droughts over India.  
 882 *Nature*, 289(5795), 271–273.
- 883 Reddy, N. N., Chakraborty, P., Roy, S., Singh, K., Minasny, B., McBratney, A. B., et al. (2021a).  
 884 Legacy data-based national-scale digital mapping of key soil properties in India.  
 885 *Geoderma*, 381, 114684.
- 886 Reddy, N. N., Chakraborty, P., Roy, S., Singh, K., Minasny, B., McBratney, A. B., et al. (2021b).  
 887 Legacy data-based national-scale digital mapping of key soil properties in India.  
 888 *Geoderma*, 381, 114684. <https://doi.org/10.1016/j.geoderma.2020.114684>
- 889 Roxy, M. K., Ghosh, S., Pathak, A., Athulya, R., Mujumdar, M., Murtugudde, R., et al. (2017a).  
 890 A threefold rise in widespread extreme rain events over central India. *Nature*  
 891 *Communications*, 8(1), 708. <https://doi.org/10.1038/s41467-017-00744-9>

- 892 Roxy, M. K., Ghosh, S., Pathak, A., Athulya, R., Mujumdar, M., Murtugudde, R., et al. (2017b).  
 893 A threefold rise in widespread extreme rain events over central India. *Nature*  
 894 *Communications*, 8(1), 708. <https://doi.org/10.1038/s41467-017-00744-9>
- 895 Roxy, M. K., Ghosh, S., Pathak, A., Athulya, R., Mujumdar, M., Murtugudde, R., et al. (2017c).  
 896 A threefold rise in widespread extreme rain events over central India. *Nature*  
 897 *Communications*, 8(1), 708. <https://doi.org/10.1038/s41467-017-00744-9>
- 898 Rumsey, C. A., Miller, M. P., Susong, D. D., Tillman, F. D., & Anning, D. W. (2015). Regional  
 899 scale estimates of baseflow and factors influencing baseflow in the Upper Colorado River  
 900 Basin. *Journal of Hydrology: Regional Studies*, 4, 91–107.  
 901 <https://doi.org/10.1016/j.ejrh.2015.04.008>
- 902 Sahana, V., Sreekumar, P., Mondal, A., & Rajsekhar, D. (2020). On the rarity of the 2015 drought  
 903 in India: A country-wide drought atlas using the multivariate standardized drought index  
 904 and copula-based severity-duration-frequency curves. *Journal of Hydrology: Regional*  
 905 *Studies*, 31, 100727. <https://doi.org/10.1016/j.ejrh.2020.100727>
- 906 Sahoo, M., & Kumar Yadav, R. (2022). The Interannual variability of rainfall over homogeneous  
 907 regions of Indian summer monsoon. *Theoretical and Applied Climatology*, 148, 1303–  
 908 1316. <https://doi.org/10.1007/s00704-022-03978-w>
- 909 Salinas, J. L., Laaha, G., Rogger, M., Parajka, J., Viglione, A., Sivapalan, M., & Blöschl, G.  
 910 (2013). Comparative assessment of predictions in ungauged basins &ndash; Part 2: Flood  
 911 and low flow studies. *Hydrology and Earth System Sciences*, 17(7), 2637–2652.  
 912 <https://doi.org/10.5194/hess-17-2637-2013>

- Sanders, K. T. (2015). Critical Review: Uncharted Waters? The Future of the Electricity-Water Nexus. *Environmental Science & Technology*, 49(1), 51–66. <https://doi.org/10.1021/es504293b>
- Schulte, J., Policielli, F., & Zaitchik, B. (2020). A skewed perspective of the Indian rainfall–El Niño–Southern Oscillation (ENSO) relationship. *Hydrology and Earth System Sciences*, 24(11), 5473–5489. <https://doi.org/10.5194/hess-24-5473-2020>
- Sen, P. K. (1968). Estimates of the Regression Coefficient Based on Kendall’s Tau. *Journal of the American Statistical Association*, 63(324), 1379–1389. <https://doi.org/10.1080/01621459.1968.10480934>
- Shah, D., & Mishra, V. (2020). Drought Onset and Termination in India. *Journal of Geophysical Research: Atmospheres*, 125(15), e2020JD032871. <https://doi.org/10.1029/2020JD032871>
- Shah, H. L., & Mishra, V. (2016). Hydrologic Changes in Indian Subcontinental River Basins (1901–2012). *Journal of Hydrometeorology*, 17(10), 2667–2687. <https://doi.org/10.1175/JHM-D-15-0231.1>
- Taylor, K. E. (2001). Summarizing multiple aspects of model performance in a single diagram. *Journal of Geophysical Research: Atmospheres*, 106(D7), 7183–7192. <https://doi.org/10.1029/2000JD900719>
- The Hindu. (2019, April 7). Looming water scarcity. Retrieved from <https://www.thehindubusinessline.com/opinion/editorial/drought-conditions-in-peninsular-india-highlight-familiar-policy-failures/article26762909.ece>
- Van Lanen, H. A. J., Wanders, N., Tallaksen, L. M., & Van Loon, A. F. (2013). Hydrological drought across the world: impact of climate and physical catchment structure. *Hydrology and Earth System Sciences*, 17(5), 1715–1732. <https://doi.org/10.5194/hess-17-1715-2013>

- 936 Van Loon, A. F. (2015). Hydrological drought explained. *WIREs Water*, 2(4), 359–392.  
 937 <https://doi.org/10.1002/wat2.1085>
- 938 Van Loon, A. F., & Laaha, G. (2015). Hydrological drought severity explained by climate and  
 939 catchment characteristics. *Journal of Hydrology*, 526, 3–14.
- 940 Wang, S., Huang, J., & Yuan, X. (2021). Attribution of 2019 Extreme Spring–Early Summer Hot  
 941 Drought over Yunnan in Southwestern China. *Explaining Extreme Events of 2019 from a*  
 942 *Climate Perspective*, 102(1).
- 943 Webster, P. J. (1981). Monsoons. *Scientific American*, 245(2), 108–  
 944 119. <https://www.jstor.org/stable/10.2307/24964541>
- 945 Wilby, R. L., Wedgbrow, C. S., & Fox, H. R. (2004). Seasonal predictability of the summer  
 946 hydrometeorology of the River Thames, UK. *Journal of Hydrology*, 295(1), 1–16.  
 947 <https://doi.org/10.1016/j.jhydrol.2004.02.015>
- 948 Wilhite, D. A. (2005). Drought. In J. E. Oliver (Ed.), *Encyclopedia of World Climatology* (pp.  
 949 338–341). Dordrecht: Springer Netherlands. [https://doi.org/10.1007/1-4020-3266-8\\_70](https://doi.org/10.1007/1-4020-3266-8_70)
- 950 Willett, K. M., Gillett, N. P., Jones, P. D., & Thorne, P. W. (2007). Attribution of observed surface  
 951 humidity changes to human influence. *Nature*, 449(7163), 710–712.  
 952 <https://doi.org/10.1038/nature06207>
- 953 Wlostowski, A. N., Molotch, N., Anderson, S. P., Brantley, S. L., Chorover, J., Dralle, D., et al.  
 954 (2021). Signatures of hydrologic function across the Critical Zone Observatory network.  
 955 *Water Resources Research*, 57(3), e2019WR026635.
- 956 WMO. (2008). *Manual on low-flow estimation and prediction. Operational Hydrology Report*  
 957 *No.50*. Geneva: WMO.



- 958 Yaeger, M., Coopersmith, E., Ye, S., Cheng, L., Viglione, A., & Sivapalan, M. (2012). Exploring  
 959 the physical controls of regional patterns of flow duration curves &ndash; Part 4: A  
 960 synthesis of empirical analysis, process modeling and catchment classification. *Hydrology  
 961 and Earth System Sciences*, 16(11), 4483–4498. [https://doi.org/10.5194/hess-16-4483-](https://doi.org/10.5194/hess-16-4483-2012)  
 962 2012
- 963 Zachariah, M., Mondal, A., Das, M., AchutaRao, K. M., & Ghosh, S. (2020). On the role of rainfall  
 964 deficits and cropping choices in loss of agricultural yield in Marathwada, India.  
 965 *Environmental Research Letters*, 15(9), 094029.
- 966 Zeri, M., Williams, K., Cunha, A. P. M. A., Cunha-Zeri, G., Vianna, M. S., Blyth, E. M., et al.  
 967 (2022). Importance of including soil moisture in drought monitoring over the Brazilian  
 968 semiarid region: An evaluation using the JULES model, in situ observations, and remote  
 969 sensing. *Climate Resilience and Sustainability*, 1(1), e7. <https://doi.org/10.1002/cli2.7>  
 970

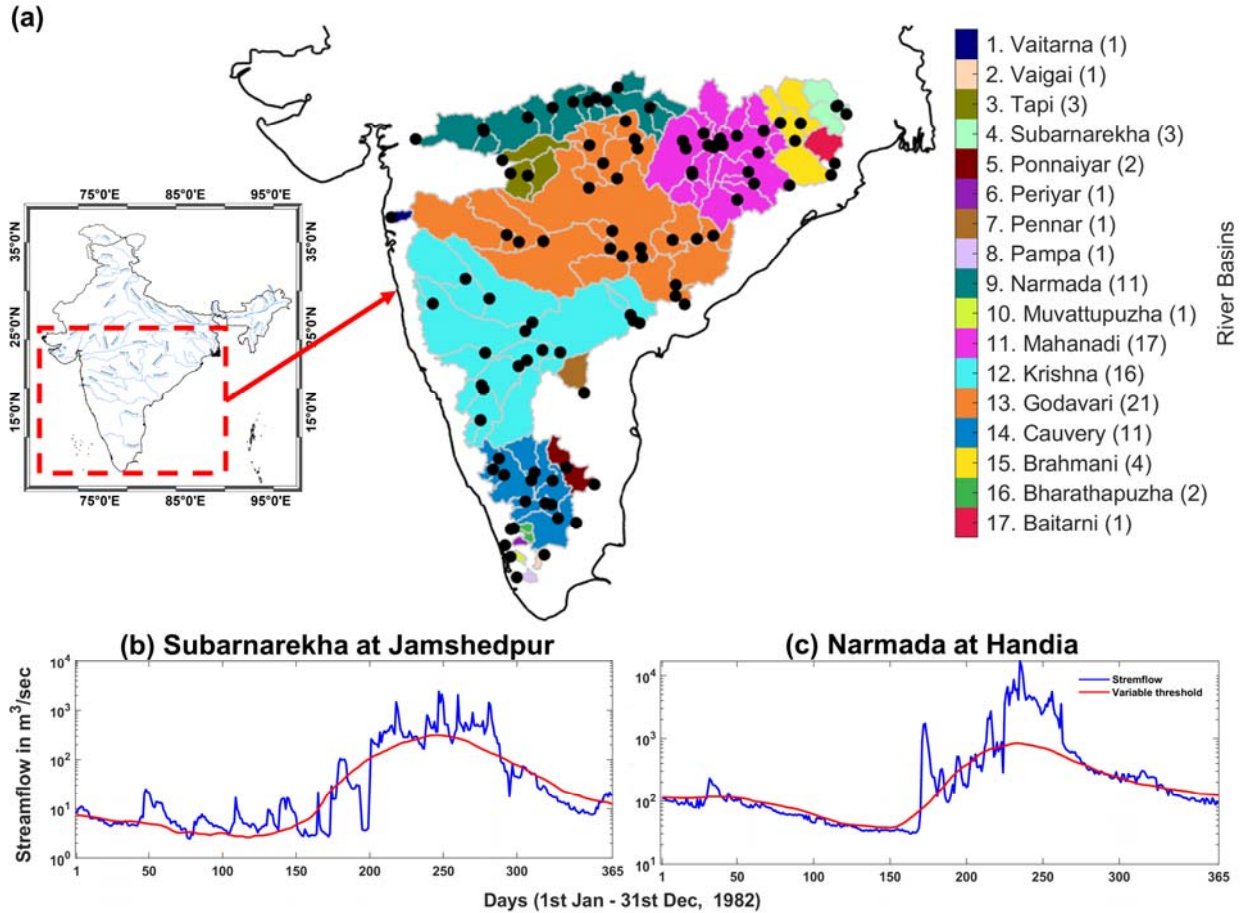


**Figure 1. Distribution of stream gauges and variable threshold approach for streamflow drought identification.** (a) Location of stream gauges over the catchments of peninsular India. Histogram shows period of record availability versus number of stations. Streamflow drought identification using daily variable threshold approach for the year 1982 at: (b) Jamshedpur station over Subarnarekha River (c) Handia gauge at Narmada River basin.

985

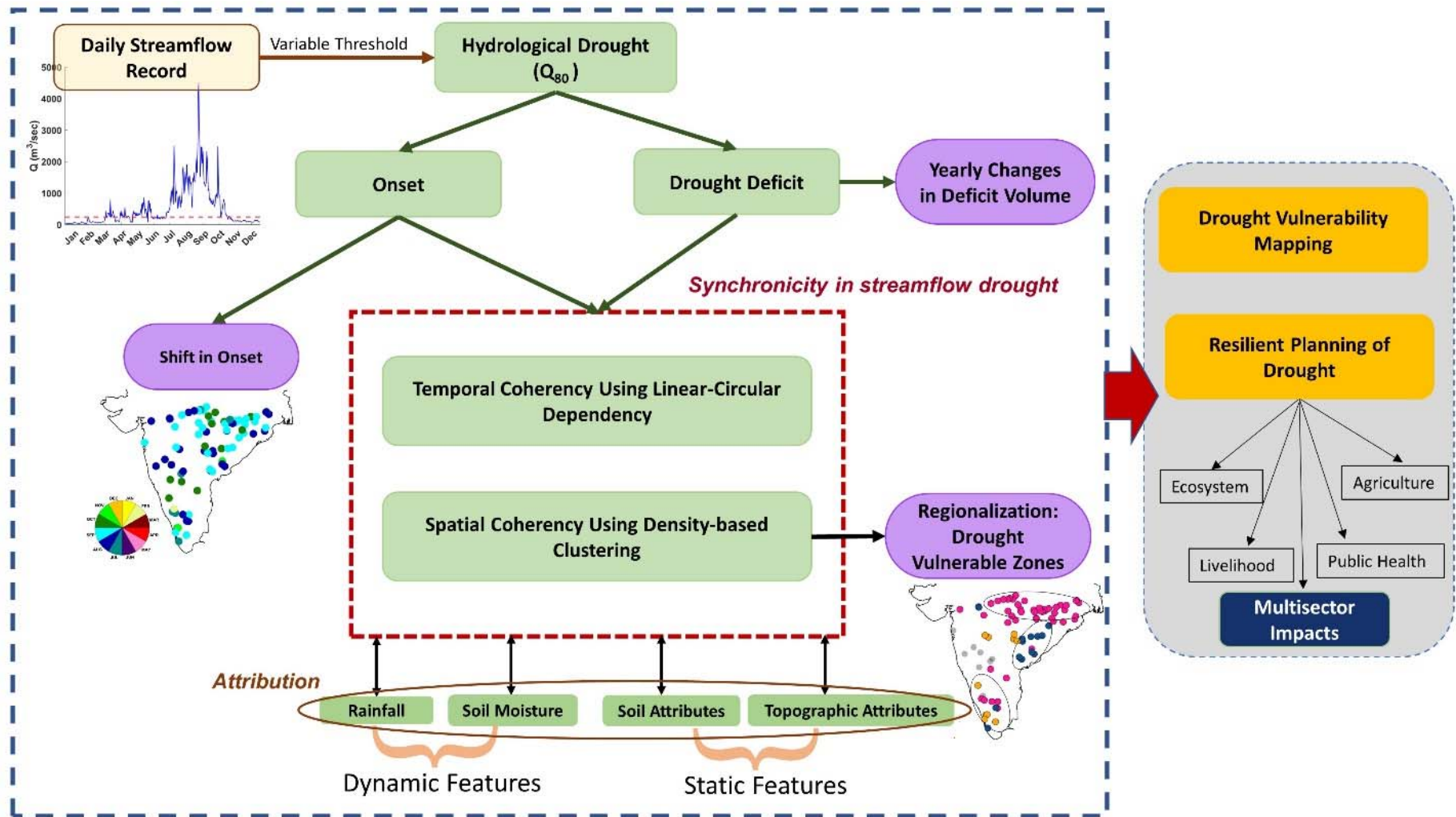
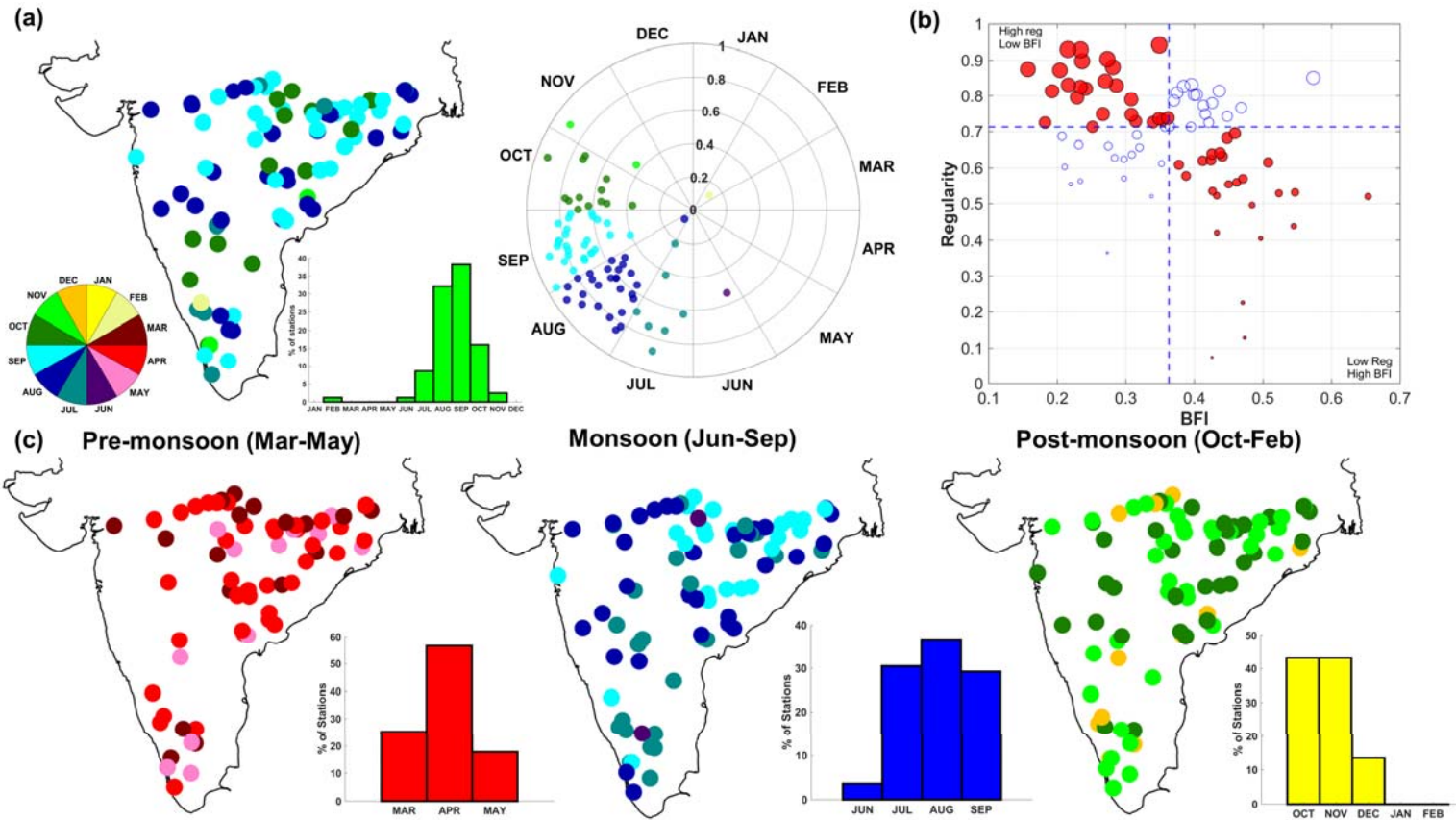


Figure 2. Overall workflow of the analysis.



989

990 **Figure 3. Trends in streamflow drought onset and regularity.** (a) (Left panel) the spatial map presenting mean onset of drought without  
 991 considering the seasonal stratifications. The shades in the pie chart in the lower-left corner show the mean timing of streamflow droughts,  
 992 whereas the histogram in the lower-right corner shows the mean onset months for gauges (in percentage). (Right panel) seasonal distribution  
 993 of regularity in the mean onset time. (b) scatter plot of regularity in mean onset time versus the Base Flow Index (BFI). The red circles  
 994 indicate significant association (with  $p < 0.1$ ) between regularity and BFI, computed using Kendall's  $\tau$ . The size of the circle increases as  
 995 the regularity increases. (c) Mean onset of drought with seasonal stratifications: (left panel) pre-monsoon: March-May, (middle panel)  
 996 monsoon: June-September, and (right panel) post-monsoon: October-February.



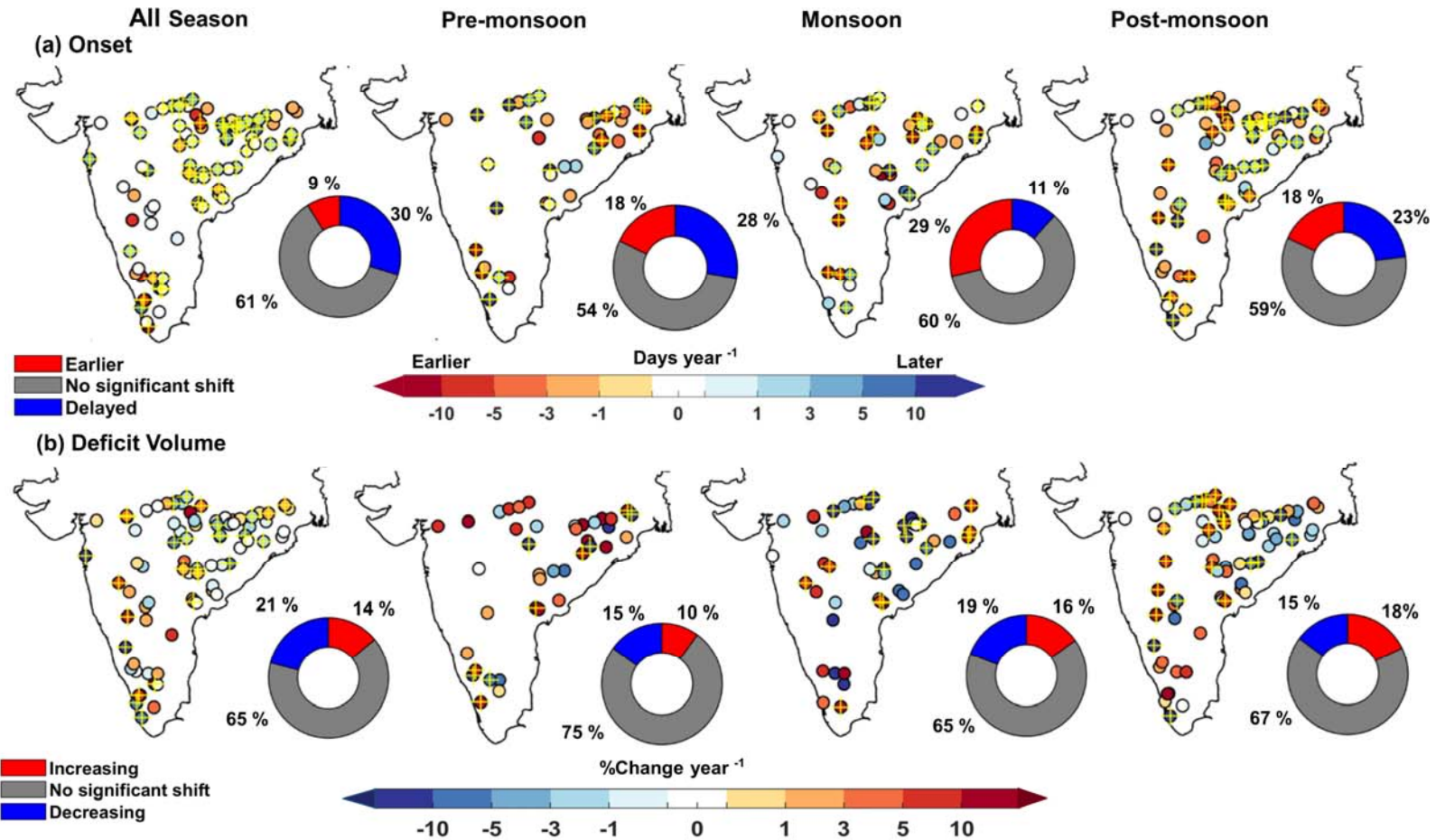
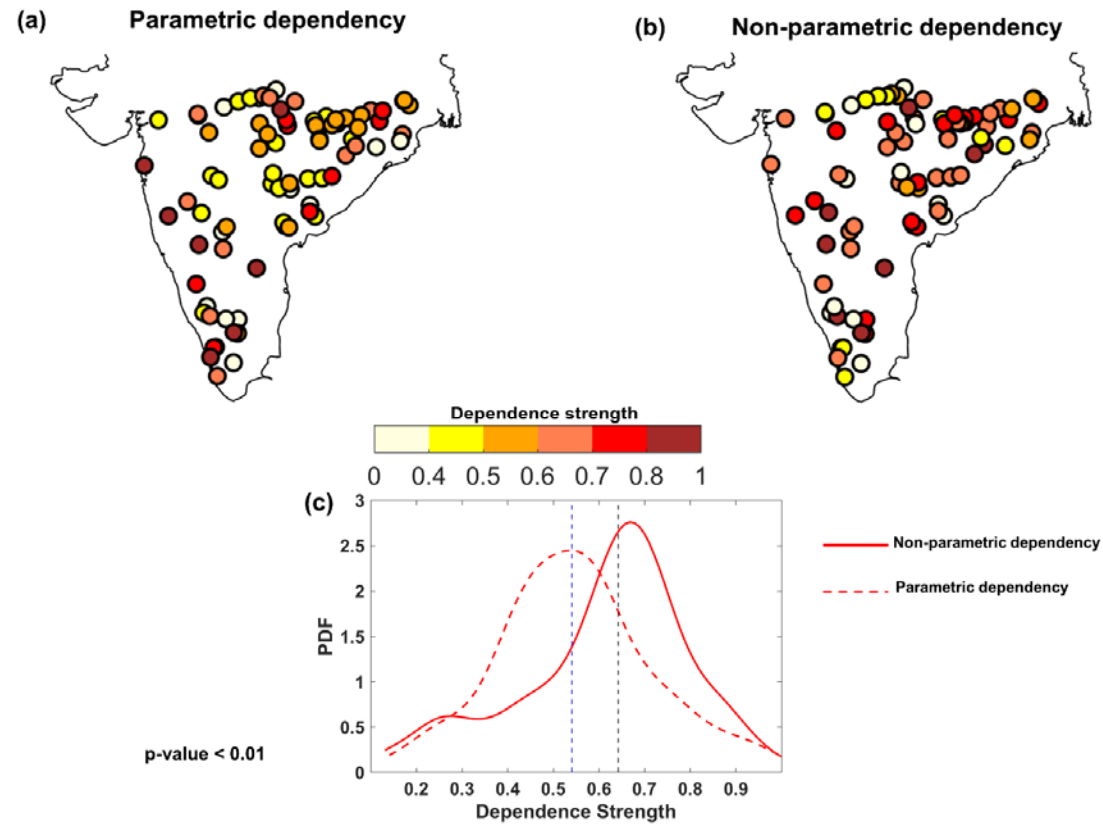


**Figure 4. Trends in drought onset and deficit volume.** (a) Trends in streamflow drought onset (days-year<sup>-1</sup>) considering without (left most panel) and with seasonal stratifications. The station with significant trend at 10 % significance level are marked with a yellow + sign. Significance in at-site trends are determined using bootstrap resampling procedure with at  $p < 0.10$  level for negative trends and at  $p > 0.90$  level for positive trends (Gudmundsson et al., 2019). The donut chart shows the fraction of stations (in %) with an earlier, delayed and no significant changes in drought onset. (b) The same as in panel (a) but for deficit volume. The donut chart shows the fraction of stations with changes in deficit volume.

1004



1005

1006 **Figure 5. Spatial footprints of dependence strengths of drought onset versus deficit volume.** Dependence between streamflow drought onset  
 1007 and deficit volume quantified using (a) Parametric method (b) non-parametric method (c) Probability density functions (PDFs) comparing  
 1008 parametric (in dotted red lines) versus non-parametric (in solid red lines) dependency. The vertical dotted lines shows median values of  
 1009 dependence strengths.

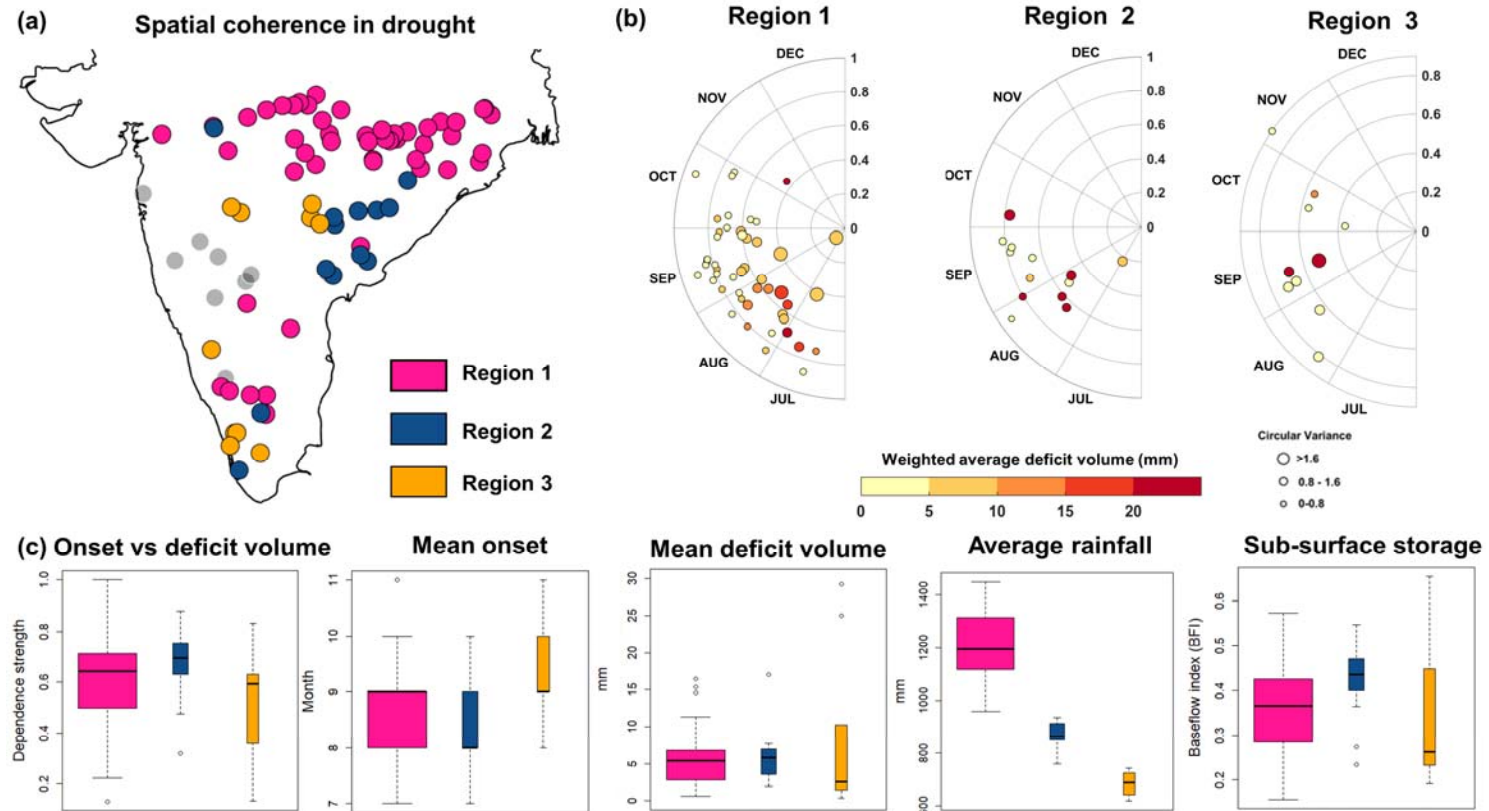


**Figure 6. Regionalization of streamflow droughts.** (a) Catchments are regionalized based on similarity measures, considering geospatial and hydrometeorological drivers using a density based clustering technique. The grey circles represent catchments that are neither part of any regions nor a border ('noise' points detected in DBSCAN). (b) Region-wise weighted average deficit volume (mm) considering duration of the event as a weighing factor. The radii along the half circles represent the regularity of drought onset – the closer the points to origin, i.e., close to zero indicates onset of drought is uniformly distributed throughout the year with no persistency in onset timing, whereas a value close to 1 indicates onset of drought clustered around the same time of the year with a high persistency in the drought onset time. The radius of each circle indicates circular variance, a measure of the dispersion of circular data. (c) Hydroclimatic drivers used for regionalization of streamflow droughts. Shades of boxplots denote each region, whereas widths vary with the number of catchments within each region. The horizontal line represents the median point at the center of the boxplot.

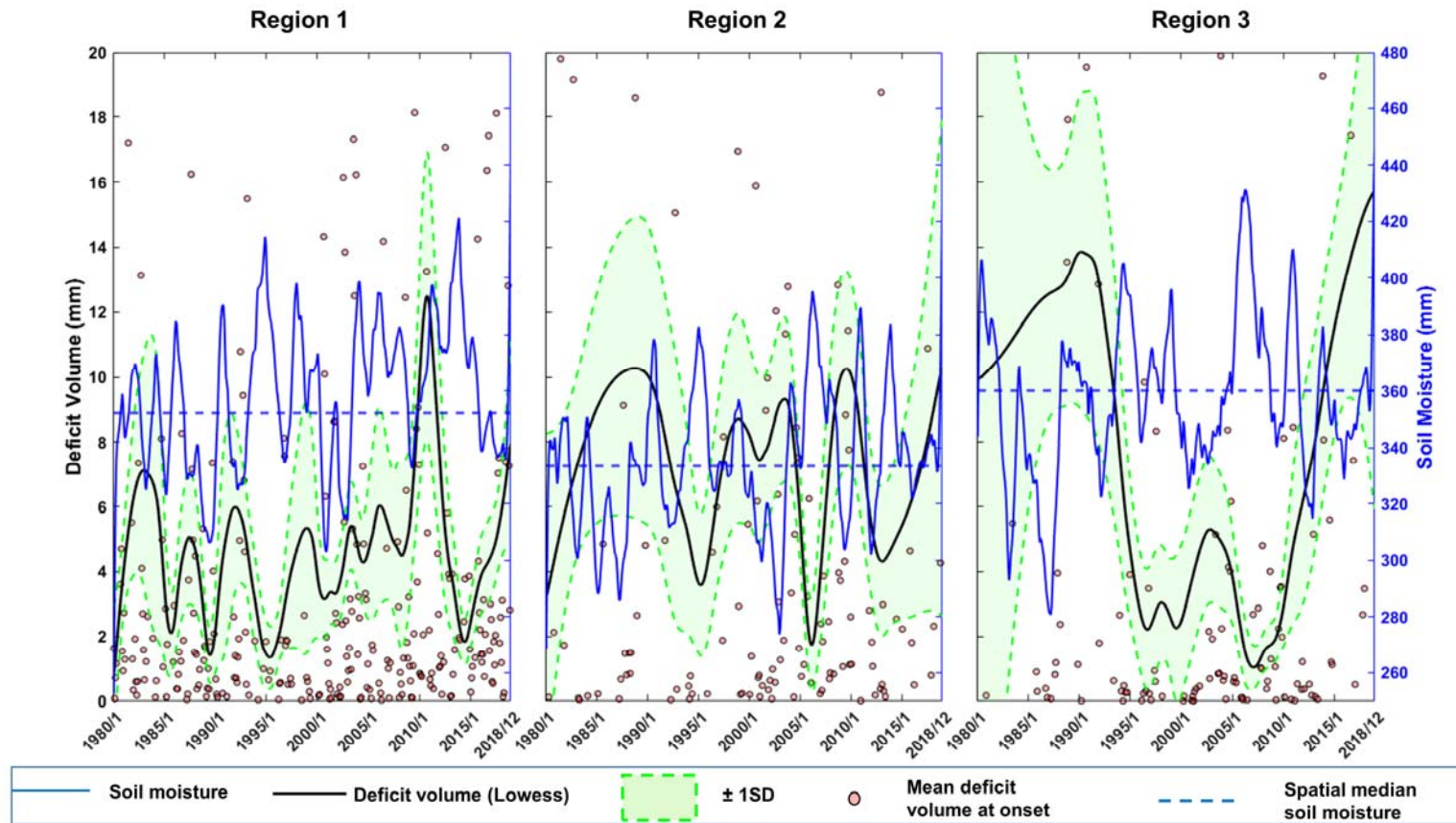
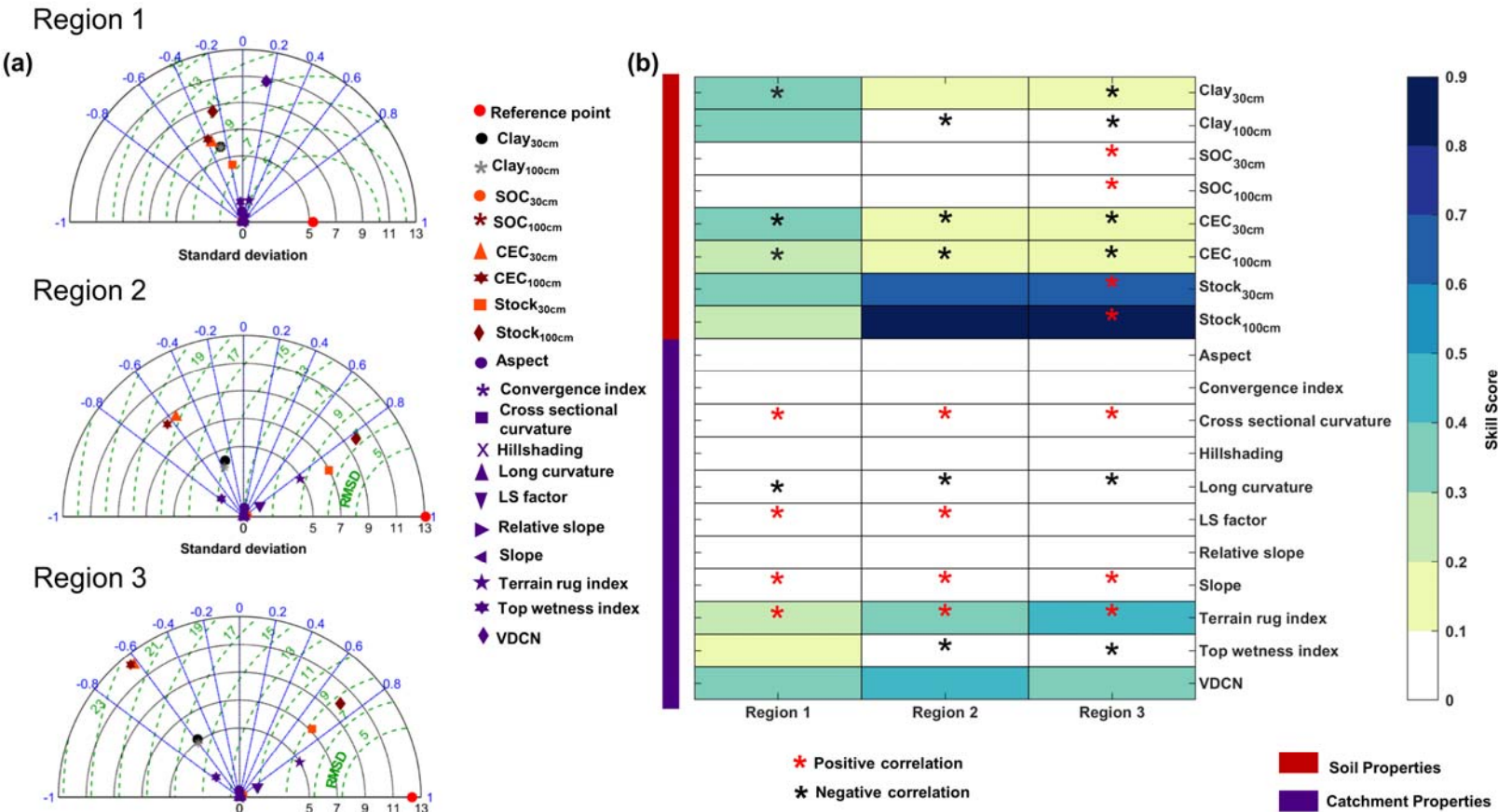


**Figure 7. Time series (1980 to 2018) comparison of soil moisture versus deficit volume.** Temporal evolution of catchment-averaged soil moisture versus drought deficit volume for each region. The (dotted) horizontal line (in blue) shows region-wise mean monthly soil moisture. The black line represents the Locally Weighted Scatterplot Smoothing (LOWESS) regression of drought deficit volume with a span length of 0.1. The uncertainty envelope (mean  $\pm 1$  standard deviation) of the LOWESS curve is obtained through 1000 bootstrap iterations. The red circles indicate individual streamflow drought events. The blue line indicates the smoothened soil moisture using a 12-month moving average filter.



1028



1029

1030 **Figure 8. Static environmental controls on drought deficit volume.** (a) Taylor diagrams illustrate the root mean square deviations  
1031 (in green dotted lines), standard deviation (in solid black lines), and centered pattern correlation coefficient (in solid blue lines).  
1032 (b) Heat maps of Taylor skill score for soil and catchment properties. The asterisks represent significant correlations at a 5%  
1033 significance level.